Universität Regensburg
Institut für Theoretische Physik

Singlet - Triplet gaps in Polymers from Range-Separated Time Dependent Density Functional Theory

Master Thesis

Birgit Kociper
under guidance of
Prof. Dr. Thomas Niehaus

Ich habe die Arbeit selbständig verfasst, keine anderen als die angegebenen Quellen und Hilfsmittel benutzt und bisher keiner anderen Prüfungsbehörde vorgelegt.
Regensburg, den 26.09.2012

Birgit Kociper

Acknowledgements

I gratefully thank Professor Thomas Niehaus for his intense support, constructive critisim and guidance during this work. Useful suggestions were provided by Professors John Lupton, Georg Schmeer and Bernhard Dick. Additionally Alexander Hupfer, Vitalij Lutsker and Chrisitan Oppenländer contributed helpful advise. I'm much obliged to Manohar Awasti for essential computational support as well as an introduction in the usage of specific computer codes and linux commands.

Contents

1 Introduction **6**

2 Theoretical Basics **8**

2.1 The Variational Principle 9
2.2 The Hartree-Fock Approximation 9
2.3 Koopmans' Theorem 11
2.4 Density Functional Theory (DFT) 12
2.5 The Kohn-Sham Approach 13
2.6 Basis Sets 15
2.7 Classification of Basis Sets 17
2.8 Exchange and Correlation Errors 18
2.9 Generalized Kohn-Sham Approach 19
2.10 Approximate XC Functionals 21
2.11 Long-Range-Corrected DFT 25
2.12 Tuning of the Range-Separation Parameter γ 26
2.13 Time Dependent Density Functional Theory 27
2.14 Asymptotic Scaling of TDDFT Matrix Elements 32
2.15 Particle-in-a-Box Model and Oscillator Strengths 33

3 Methodology and Results **36**

3.1 Input from the Experiment 36
3.2 Simplified Polymers 39
3.3 Planar vs. Twisted Structures 42
3.4 Computational Details 44
3.5 Performance Prognosis of the used Functionals 45
3.6 Ordering of the two lowest Singlet States 46
3.7 Excitation Energies and the Spectra 48
3.8 LRC Parameter Scaling 51
3.9 Results from Absorption Energies 52
3.10 Transition Energies 55
3.11 Localization Behavior 61
3.12 Discussion of the Deviating Results 68

4 Summary and Outlook **70**

5 Appendix **72**

5.1 Polymer 2 (Triphenylene) 73
5.2 Polymer 3 74
5.3 Polymer 4 75
5.4 Polymer 5 76
5.5 Polymer 6 77
5.6 Excitation Energy Comparison of Planar and Twisted Geometries 78
5.7 Energies, Oscillator Strengths and Orbital Mixing of the Two Lowest Excited Singlet States 78

References **80**

1 Introduction

Today, most quantum mechanical theoretical research in condensed matter physics and chemistry deals with solving the Schrödinger equation for many body problems. Fundamental interactions and basics laws are included in a well-known Hamiltonian that describes the system. However an analytical solution for more than two electrons is not possible[1] and even the numerical exact solution of more than 10 electrons can not be dreamt of. Even if time dependence is put aside, the computational demand for finding the ground state grows exponentially with the number of electrons. Moreover, the full wavefunction Ψ contains far more information than one would want to know.[2]

Let's assume we want to store the ground state of one oxygen atom, by disregarding spin. The wavefunction includes 8 electrons and depends therefore on $3 \cdot 8$ coordinates. A coarse grid with ten points for each coordinate would require 10^{24} numbers to represent the wavefunction. If each number needs one byte to store, we would need 10^{14} DVD's with a capacity of 10 GB each to store just the ground-state wavefunction of one atom. But the properties we are interested in are integrated quantities like probability densities which can be extracted from Ψ.[3]

Therefore, it is often more appropriate to reformulate the problem, make it suitable for a reduced problem and use then approximations to describe the difference to the full ansatz. Ideally, the calculation and the analysis of the desired properties is simplified.

In order to deal with many-body problems and interactions, some wavefunction based approximations had been developed. One of these is the Hartree-Fock approach, which treats each electron independently and uses an average field to describe the other electrons and the nuclei. However, it neglects electron correlation (explicit electron interactions). Some methods that try to recover this missing correlation are Moller-Plesset perturbation theory (MP), configuration interaction (CI) and coupled-cluster (CC).[4]

Conceptually different is the density functional theory (DFT) approach, which emerges the electron density as a fundamental quantity. It by-passes the need to calculate Ψ or explicit forms of the Hamiltonian directly what makes it highly attractive. The exponential scaling with the system-size is in time dependent DFT replaced with a much lower N^3 or N^2 scaling, depending on the implementation.[3],[5] As the performance of computers is steadily growing, this spawned a new field in chemistry and physics - computational science. Computers are now used as 'experimental tools' - like e.g. an NMR spectrometer. Nanoscale devices or molecules can be studied and compared to 'real' experiments.[3]

The experimental context of this work are luminescent conjugated polymers. Even though

light emitting polymers were reported first in 1990, the relevance of them was discovered mainly after the Nobel Prize for Chemistry in 2000. Alan Heeger, Alan MacDiarmid and Hideki discovered that 'doped' polyacetylene can be an conductor. This led to major advances in plastic electronics like electroluminescent polymers and commercial applications in light-emitting devices. The active units in light emitting devices (LEDs) in display applications consisted usually out of inorganic phosphors, available since the early 1960s. Due to the plastic electronic improvements, within the past decade, organic LEDs (OLEDs) have become popular in commercial applications.[6]

In order to control particular properties of these organic emitters by synthesis, first principle research is performed to yield the particular 'recipe' on how to get certain desired properties. One quantity, that is relevant to 'tune', is the singlet-triplet gap of conjugated polymers as a small gap could lead to a higher emitter efficiency.[7] Usually electrical injection of charges into an OLED leads to singlet and triplet excitations where the decay of the latter is mostly non-radiative. To promote radiative triplet recombination, usually heavy-atom centers are employed to promote spin-orbit coupling, leading to a higher phosphorescence probability.[8] Triphenylene and some other polycyclic aromatic hydrocarbons are an exception: the phosphoresce from the triplet state is observed at low temperatures without incorporation of heavy atoms.[9]

The tuning of the singlet-triplet gap of polymers by choosing different types of triphenylene based polymers was performed by Lupton et. al.[9] The goal of this work is to reproduce these results by means of time dependent DFT (TDDFT). Additionally the experiment indicates, that the first singlet excited state is delocalized, whereas the triplet state shows localization - this information shall also be gained by TDDFT. The implicit reason in the experiment are phosphorescent energies which are nearly constant whereas the fluorescence differs for each system. In TDDFT these localization effects can be checked not only implicitly by also explicitly based on the relaxed excited state molecular geometry.

However, the TDDFT codes can't be used as a 'black box' because the reliability of the results depends not only on the functional and the basis set used, but also on the molecule class, the type of the investigated excited state and the use of further approximations. Therefore we account for each of these additional sources of error and use different approaches. The relatively new and promising range-separated functionals[10] are compared to standard functionals. These are based on the observation, that only methods using full Hartree-Fock exchange describe the distance dependence of long-range charge-transfer energies correctly.[11] The results for non-charge-transfer states can be improved as well.[10]

2 Theoretical Basics

In this section, the basic principles used in Density Functional Theory (DFT) describing many-body problems both for the time dependent and time independent properties of a quantum mechanical system will be introduced. The variational principle is used to determine the ground state energy in the Hartree-Fock approximation which accounts for the average electron-electron interaction. From this subsequently follows Koopman's theorem, connecting the ionization potential with the highest occupied molecular orbital. In the next subsection density functional theory is introduced intuitively and formally. The successful method of a fictitious Kohn-Sham system of non-interacting electrons yields the famous Kohn-Sham equations describing the practical approach to solve many-body problems by means of DFT.
In order to perform the calculations on a computer, the theoretical infinite basis sets have to be truncated to a finite set of basis functions where different atomic orbital sets can be used. After the overview of these basis sets, they are classified by their size and higher angular momentum structures. As the functionals of DFT are always approximations yielding errors for the exchange and correlation part, the question on how to improve on these errors is discussed. This leads to the introduction of the so called 'Generalized Kohn-Sham' approach which differs from the conventional KS approach. It uses a non-local potential leading to different orbitals but yielding in principle the ground state energy and density of the exact interacting system. It is shown that whereas Koopman's Theorem is an approximation in HF theory, in GKS this relations holds exactly due to the presence of correlation. Next, different approximate exchange-correlation (XC) functionals are explained schematically as these functionals are the key element in DFT - all interaction problems of a many-body system are 'outsourced' to these functionals and potentials. As conventional XC potentials show a wrong long range behavior, the promising long range corrected XC functionals are introduced. These compensate the wrong behavior, the Coulomb operator is partitioned into a short-range and a long-range part and weighted with a parameter function γ. The quality of this separation method depends then vitally on the choice of γ. In the next subsections the theorem and the methods behind the time-dependent DFT (TDDFT) which lead to time-dependent Kohn-Sham equations are described. TDDFT is an independent approach relying on a similar theorem than in DFT, but the key factor is the time-dependent potential which is a functional of the time dependent density. The last subsections specifies, how the range-separation parameter γ should be tuned in order to optimize the results of a calculation.

2.1 The Variational Principle

For a hamiltonian $\hat{H}$ that describes a studied system and any normalizable test function ψ with arguments appropriate for the unknown wavefunction of the system, we define the functional[12]

$$E[\psi] = \frac{\langle\psi|\,\hat{H}\,|\psi\rangle}{\langle\psi|\,\psi\rangle}. \tag{1}$$

The Rayleigh-Ritz variational principle states that

$$E_0 \leq E[\psi] \tag{2}$$

where E_0 is the ground state of $\hat{H}$. One has to distinguish a *functional* like the energy in Eq. (1) from a *function* like the density or a wavefunction. A *functional* is a mapping routine that extracts properties from a function, which in turn depend on variables. A functional will therefore be denoted with $F[f]$, while $f(x)$ is the common notation of a function.
The variation of $|\psi(\mu)\rangle$ trough the parameter μ leads to a minimum search of $E(\mu)$. This minimal energy is then an upper limit for the ground state energy. The exact ground state energy is only obtained if the wavefunction is equal to that of the exact system.
In order to study molecular systems, we can write the minimization in the following form, using the Born-Oppenheimer approximation[13] for $\hat{H}$:[16]

$$E_0 = \min\left(E[\psi]\right) = \min\left(\langle\psi|\,\hat{T} + V_{\text{ee}} + V_{\text{ext}}\,|\psi\rangle\right) \tag{3}$$

where ψ is an allowed N-particle wavefunction, V_{ee} is the electron-electron interaction and V_{ext} is the external potential, for example the potential of the atomic cores. The variational principle is used e.g. for molecule geometry optimizations. Any approximate wavefunction will have an energy above or equal to the exact ground state energy. The wavefunction yielding the lowest energy, which is found via minimization of the ground state energy is used in an self consistent cycle to determine the molecular geometry at the energy minimum.

2.2 The Hartree-Fock Approximation

This and the next subsection is mainly a summary of the Hartree-Fock subsection of the Book "Introduction to Computational Chemistry" of Jensen.[1]

In the Hartree-Fock (HF) approximation the wavefunction is defined by the antisymmetrized Slater determinant Φ of N one-electron wavefunctions (spin-orbitals) ϕ_i:

$$\begin{gathered}\Phi = \hat{A}[\phi_1(1)\phi_2(2)...\phi_N(N)] \\ \hat{A} = \frac{1}{\sqrt{N!}}\sum_{p_0}^{N-1}(-1)^p\hat{P} = \frac{1}{\sqrt{N!}}\left[\mathbb{1} - \sum_{ij}\hat{P}_{ij} + \sum_{ijk}\hat{P}_{ijk} - ...\right]\end{gathered} \tag{4}$$

where $\hat{A}$ is the antisymmetrization operator, which is expanded as a sum of permutations p ($\hat{P}$ is the permutation operator, yielding all possible permutations of the number of electron coordinates given as index). The variational principle is then used to determine the HF Energy E:

$$E = \min(E[\psi]) \tag{5}$$

with

$$E[\psi] = \sum_{i=1}^{N}\hat{h}_i + \frac{1}{2}\sum_{i,j=1}^{N}(\hat{J}_{ij} - \hat{K}_{ij}) \tag{6}$$

where $\hat{h}_i$ is the part originating from the one-body operators whereas $\hat{J}_{ij}$ and $\hat{K}_{ij}$ contributes for the two-body operators. By expressing the energy in terms of operators, the form of the Coulomb ($\hat{J}$, second term) and exchange ($\hat{K}$, third term) operators are specified

$$\begin{gathered}E = \sum_{i}^{N}\langle\phi_i(1)|\,\hat{h}_1\,|\phi_i(1)\rangle + \\ \frac{1}{2}\sum_{i,j=1}^{N}(\langle\phi_i(1)\phi_j(2)|\,\frac{1}{|\hat{\mathbf{r}}_1 - \hat{\mathbf{r}}_2|}\,|\phi_i(1)\phi_j(2)\rangle - \langle\phi_i(1)\phi_j(2)|\,\frac{1}{|\hat{\mathbf{r}}_1 - \hat{\mathbf{r}}_2|}\,|\phi_j(1)\phi_i(2)\rangle\end{gathered} \tag{7}$$

As the Coulomb 'self-interaction' $\hat{J}_{ii}$ and the corresponding 'exchange' element $\hat{K}_{ii}$ are the same, they cancel each other leading to an important error cancelation for self-interactions. The best set of orbitals ψ_i is determined by the variational principle. The variation of the energy can be written in terms of the Fock operator $\hat{F}_i$.

$$\hat{F}_i = \hat{h}_i + \sum_{j=1}^{N}(\hat{J}_{ij} - \hat{K}_{ij}) \tag{8}$$

Using Lagrange multipliers λ_{ij}, the final set of Hartree-Fock equations may be written as

$$\hat{F}_i\phi_i' = \sum_{j}^{N}\lambda_{ij}\phi_i'. \tag{9}$$

An unitary transformation yields $\lambda_{ij} = 0$ and $\lambda_{ii} = \epsilon_i$ which transforms this to

$$\hat{F}_i \phi_i = \epsilon_i \phi_i \tag{10}$$

where $\epsilon_i = \langle \phi_i | \hat{F}_i | \phi_i \rangle$ are the orbital energies, which can be calculated easily for occupied orbitals as well as for unoccupied ones.
HF theory accounts for the average electron-electron interaction and the exchange energy is exact, but it neglects the correlation between electrons. This would require a multi-determinant wavefunction whereas HF theory is based on a single-determinant wavefunction.[1]

2.3 Koopmans' Theorem

From Eq. 6, directly follows that the ionization potential (IP) is simply given by the orbital energy of the highest occupied molecular orbital (HOMO) known as Koopmans' theorem:

$$IP = E_{N-1} - E_N = -\epsilon_{HOMO}. \tag{11}$$

This is only valid if the molecular orbitals are considered constant for a N and a N-1 electron system (frozen MO's). Similarly, in this approximation, the electron affinity (EA) is given as the energy of the lowest unoccupied molecular orbital (LUMO):

$$EA = E_N - E_{N+1} = -\epsilon_{LUMO}. \tag{12}$$

However, the method to determine the EA is questionable, as it takes unoccupied orbital energies which are not always well defined with respect to convergence behavior. In contrast eigenvalues of occupied orbitals converge to a finite value if the basis set size is increased. The deeper rooted problem with the electron affinity is that in DFT ϵ_{LUMO} will never estimate the exact EA value - even if the exact potential would be used. This is due to derivative discontinuities of the exchange-correlation energy.[14]
Koopmans theorem in HF is an approximation because the MO's are not relaxed when the charge is added or removed and additionally the HF treatment which yields the energy for $\epsilon_{HOMO/LUMO}$ includes no correlation.[1]

2.4 Density Functional Theory (DFT)

The next two subsections are mainly a summary of the DFT chapter in the Book of Jensen,[1] the TDDFT Review by P. Elliott et. al[16] and the TDDFT Lecture Notes of Gross and Burke.[17]
The electron density $\eta(\mathbf{r}, t)$ is the core of the DFT and is defined as the probability density of finding an electron at position $\mathbf{r}$ at time t:

$$\eta(\mathbf{r}, t) = N \int d^3\mathbf{r_2} \cdots \int d^3\mathbf{r_N} \ \left|\psi(\mathbf{r_1}, \mathbf{r_2}, ..., \mathbf{r_N}, t)\right|^2, \tag{13}$$

where N is the number of electrons in the system. In DFT one minimizes energy functionals of the electron density in order to get approximate solutions for many body systems.[18], [19] The 'intuitive' arguments for the one-to-one correspondence between the electron density of a system and the energy had been summarized by E.B. Wilson,[20] who argued that:

- The integral of the density defines the number of electrons.
- The cusps in the density define the position of the nuclei.
- The heights of the cusps define the corresponding nuclear charges. This defines the density and therefore in principle the many-body wavefunction.

The formal justification of these ideas were stated by Hohenberg and Kohn in 1964.[21] The first theorem states that the electron density of a non-degenerate ground state uniquely determines the Hamiltonian and thus all properties of the system. Later it was shown that this also holds for degenerate ground states[22] and analogous theorems could be applied to spin densities, η_α, η_β with $\alpha, \beta \in \{|\uparrow\rangle, |\downarrow\rangle\}$. That means that the external potential V_{ext} is (to within a constant) a unique functional of $\eta(r)$, the ground state density. The ground state energy can therefore be written as a functional of the density

$$E[\eta] = E_{\text{ext}}[\eta] + T[\eta] + E_{\text{ee}}[\eta] = \int d^3r \, V_{\text{ext}}(\mathbf{r})\eta(\mathbf{r}) + F_{HK}[\eta], \tag{14}$$

with $T[\eta]$ is the kinetic energy functional and E_{ee} the electron-electron interaction. We split the problem into one part which is system specific and one part which is universal but not known and call it F_{HK}. If we have good approximations for these terms, we obtain the density, as it is justified by the second Hohenberg-Kohn theorem. It says, that the total energy density functional delivers its lowest energy for the exact ground state density. This can be easily verified by use of the variational principle.

The success of modern DFT methods is based on a fictitious Kohn-Sham (KS) system[23] of non-interacting electrons with the same spin densities. If the HK theorem is applied to this system, the potentials $V[n_\alpha, n_\beta]$ are gained, which give the ground state spin densities. The approach to map the fully interacting problem to the auxiliary KS System is described in the following.

2.5 The Kohn-Sham Approach

In order to calculate the electronic ground-state energy from the minimum principle (by searching over all normalized, antisymmetric N-electron wavefunctions ψ),

$$E_{gs}[\eta, N] = \min_{\psi \to N}[\langle\psi|\,\hat{H}\,|\psi\rangle] \tag{15}$$

the Kohn-Sham approach uses a fictitious Hamiltonian operator of the following form, with $0 \leq \lambda \leq 1$

$$\hat{H}_\lambda = \hat{T} + \hat{V}_{\text{ext}}(\lambda) + \lambda\hat{V}_{\text{ee}} \tag{16}$$

where $\hat{V}_{\text{ext}}(\lambda)$ is equal to $\hat{V}_{\text{ne}}$, the nuclear-electron interaction for $\lambda = 1$. For smaller values of λ it is assumed that $\hat{V}_{\text{ext}}(\lambda)$ is adjusted such that the *same* density is obtained for $\lambda = 1$ (real system) as for all other λ values ($\lambda = 0$ for the fictitious system with non-interacting electrons). This approach just shifts all problems to the modulation of the external potential. For $\lambda = 0$, the exact solution of the Schrödinger equation is given as a Slater determinant (denoted by subscript S) of molecular orbitals $\psi_{i\sigma}$ where the exact kinetic energy is known as

$$T_S = -\frac{1}{2}\sum_\sigma \sum_i^{N_\sigma} \langle\psi_{i\sigma}|\,\vec{\nabla}^2\,|\psi_{i\sigma}\rangle\,, \tag{17}$$

where N_σ is the total number of spin-up or spin-down electrons respectively. Here we use atomic units (a.u.) which are defined by setting $m_e = e = \hbar = 1$ (related quantities of these units can be found in Appendix C in Ref.[1]). This kinetic energy under the assumption of non-interacting electrons is the key element in KS theory. The remaining kinetic energy in real systems with interactions is shifted into an exchange-correlation term. With this a general DFT energy expression is:

$$E[\eta] = T_S[\eta] + \int d^3r\, V_{\text{ext}}(\mathbf{r})\eta(\mathbf{r}) + J[\eta] + E_{XC}[\eta], \tag{18}$$

with the so-called exchange-correlation functional which is *defined* by comparison of the latter equation with the energy of real system in Eq. (14):

$$E_{XC}[\eta] \coloneqq (T[\eta] - T_S[\eta]) + (E_{ee}[\eta] - J[\eta]), \tag{19}$$

where $J[\eta]$ accounts for the electron-electron correlation.
After applying the variational principle and taking both spin densities into account, we can put all the unknown potentials together into V_{eff}:

$$\frac{\delta E[\eta_\alpha, \eta_\beta]}{\delta \eta_\sigma(\mathbf{r})} = \frac{\delta T_S[\eta_\alpha, \eta_\beta]}{\delta \eta_\sigma(\mathbf{r})} + \underbrace{V_{\text{ext}}(\mathbf{r}) + \sum_{\sigma'} \int d^3r' \, \frac{\eta_{\sigma'}(\mathbf{r}')}{|\mathbf{r} - \mathbf{r}'|} + V_{XC}^{\sigma}(\mathbf{r})}_{V_{\text{eff}}}, \tag{20}$$

where the second term in V_{eff}, denotes the Hartree term and the exchange-correlation(XC) potential is given by the functional derivative of the XC energy

$$V_{XC}^{\sigma}(\mathbf{r}) = \frac{\delta E_{XC}[\eta_\alpha, \eta_\beta]}{\delta \eta_\sigma(\mathbf{r})}. \tag{21}$$

This connects the KS system with the physical problem. The uncontrollable many-body problem of interacting electrons in a static external potential is reduced to a controllable problem of non-interacting electrons moving in an effective potential. The hamiltonian for such a system reads

$$\hat{H} = -\frac{1}{2} \sum_i^N \vec{\nabla}_i^{\,2} + \sum_i^N V_{\text{eff}}(\mathbf{r}_i) \tag{22}$$

and the eigenwert problem which is called Kohn-Sham equation, is solved by single-body wavefunctions satisfying:

$$\left(-\frac{1}{2}\nabla^2 + V_{\text{eff}}^{\sigma}(\mathbf{r}) \right) \psi_{i\sigma}(\mathbf{r}) = \epsilon_{i\sigma} \, \psi_{i\sigma}(\mathbf{r}). \tag{23}$$

These orbitals $\psi_{i\sigma}(\mathbf{r})$ reproduce the desired spin-dependent density $\eta(\mathbf{r})$ of the original many-body system:

$$\eta_\sigma(\mathbf{r}) = \sum_i^{N_\sigma} |\psi_{i\sigma}(\mathbf{r})|^2. \tag{24}$$

Unlike the Hartree-Fock approximation, DFT is not an approximation because it gives an exact answer if V_{XC} is exactly known. Unfortunately, the exchange and correlation functionals are not known except for the free electron gas. However, approximations exist

which permit the calculation of certain physical quantities quite accurately - much better than with Hartree-Fock. The exact or approximated $E_{XC}[\eta_\alpha, \eta_\beta]$ can be differentiated to get V_{XC} what self-consistently reproduces the spin-densities, orbitals and total energies by inserting it again into Eq. (20). This self-consistent cycle is then repeated until convergence is reached.

2.6 Basis Sets

This subsection is mainly a summarization from Ref.[1] For the practical implementation of DFT in calculations, one has to solve the Kohn-Sham equations (23). To do so, a common approach is to expand the orbitals $\psi_i(\mathbf{r})$ into a finite set of basis functions[16]

$$\psi_{i\sigma}(\mathbf{r}) = \sum_{\mu}^{L} c_{\mu i\sigma}\ \phi_\mu(\mathbf{r}) \tag{25}$$

which leads to a generalized eigenvalue equation of dimension L

$$\sum_{\nu}^{L} H^{DFT}_{\mu\nu\sigma}[\eta]\, c_{\nu i\sigma} = \sum_{\nu}^{L} \epsilon_{i\sigma}\, S_{\mu\nu}\, c_{\nu i\sigma} \tag{26}$$

with $\hat{H}^{DFT}_{\mu\nu\sigma}[\eta] = \int d^3r\, \phi_\mu(\mathbf{r})\, \hat{H}^{DFT}_{\sigma}[\eta]\, \phi_\nu(\mathbf{r})$ and the overlap matrix $S_{\mu\nu} = \int d^3r\, \phi_\mu(\mathbf{r})\, \phi_\nu(\mathbf{r})$. This equation can be easily solved by means of standard linear algebra with a computer, if one knows $H^{DFT}_{\mu\nu}$ and $S_{\mu\nu}$. We therefore need good approximations for the basis sets $\phi_\mu(\mathbf{r})$.
For molecules, surfaces and solids, the linear combination of atomic orbitals (LCAO) $\phi_\mu(\mathbf{r} - \mathbf{R}_A)$ works quite well. There are three main types of atomic orbital sets, which will be explained in the following.

- **Gaussian Type Orbitals (GTO)**
  GTOs are the most common choice - the basis functions are atom-centered and have the form
  $$\phi(x, y, z) = N\, x^l y^m z^n\, e^{-\alpha r^2} = N\, r^L\, e^{-\alpha r^2} \tag{27}$$
  with $r = \sqrt{x^2 + y^2 + z^2}$ and the quantum number $L = l + m + n$ which is used to classify the GTO into s/p/d - functions corresponding to L=0/1/2.

- **Slater Type Orbitals (STO)**

Another common basis functions are Slater type orbitals given by

$$\phi(r,\theta,\phi) = N\, r^{n-1} e^{-\beta r}\, Y_{lm}(\theta,\phi), \tag{28}$$

where the angular part is given by spherical harmonics $Y_{lm}(\mathbf{r})$ depending on the polar coordinates of the position vector $\mathbf{r}$ and the radial part is exponentially decaying. Here N is a normalization constant and n is the principle quantum number, $n = 1, 2, ...$

The advantage of STOs is that they represent the behavior of the wavefunction at $r = 0$ much better than GTOs which have a zero slope at the nucleus. Moreover a GTO drops off too rapidly far from the nucleus compared to an STO. But the disadvantage of STOs is, that products of two STOs on distinct atoms are more difficult to express than with GTOs.

In order to combine the advantages of both types, one can use linear combinations of GTOs (so-called **Constructed Gaussian functions (CGF)**) which try to approximate a certain Slater type function:

$$\phi_\tau^{CGF}(\mathbf{r}) = \sum_a^A d_{a\tau}\, \phi_a^{GTO}(\mathbf{r}). \tag{29}$$

The individual GTO are called primitive GTOs. A rough guideline is that there are three times as many GTOs as STOs needed to reach a given level of accuracy. Schematically this is shown in Fig. 1 where a STO is modeled by a linear combination of GTOs.

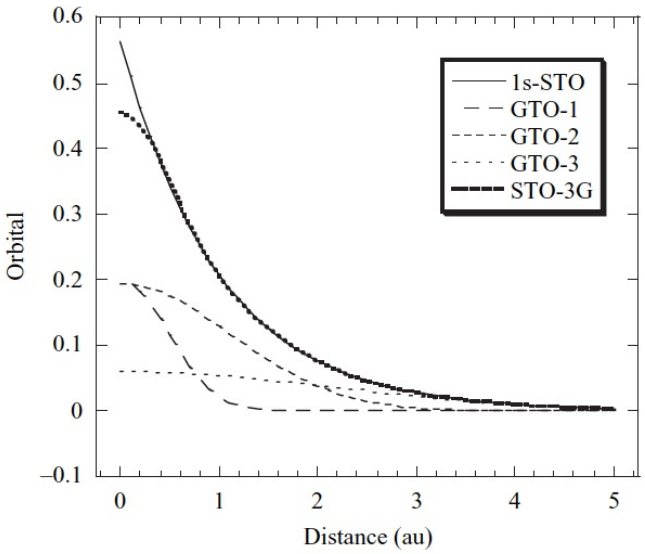

Figure 1: A 1s-STO is modelled by a linear combination of three GTOs (STO-3G); from Ref.[1]

Yet, in terms of computational efficiency, the higher number of GTO functions is still compensated because the GTO integrals are faster to compute as they reduce the dimension of the Hamiltonian.

- **Numerical Orbitals**
  Atomic orbitals can also be pre-calculated numerically, which reduces the computational effort in DFT calculations. This is used in the DFTB computer codes (Density Functional based Tight Binding). Here the molecular basis set is given by data points on a grid, where each type of integral requires a numerical integration.

2.7 Classification of Basis Sets

After choosing the type of basis function, the question is how many of those basis functions one needs to obtain a good accuracy. The trial and error method is to increase systematically the basis set size and compare the results to the experimental values. The following classification of basis sets follows Ref.[1]
The smallest possible basis is a so-called **Minimal basis set**, where only *occupied* atomic orbitals are represented by a single basis function. Examples are the so-called STO-nG, where n is an integer representing the number of primitive GTOs used to approximate one STO basis set. Minimal basis sets give only rough results.

By doubling all basis functions of the minimal basis set (e.g. 1s and 1s' for hydrogen) one gets a **Double Zeta** (DZ) type basis. The name zeta origins from the greek letter exponent of the STO basis function, often denoted by ζ. This basis set is an improvement to STOs as it allows to describe asymmetric bondings (different bondings in different directions). As the chemical bonding occurs between valence orbitals, the doubling usually refers to the doubling of valence orbitals (split valence basis) as the doubling of core orbitals is rarely considered in actual calculations. The next steps on the ladder are Triple Zeta, Quadruple Zeta, etc. basis sets following the same logic. In addition to the first set of polarization (p-) functions corresponding to the occupied orbitals, higher angular momentums are also quite important. These can be included by adding p-functions on hydrogens and d-functions on heavy atoms. This is denoted with DZP, TZP,... and DZ2P, TZ2P if two sets of polarization functions are added.
Another commonly used type of split-valence basis sets is notated with *k-nlmG*, where *k* indicates how many GTOs are used to represent the atomic core orbitals. The *nlm* deliver two information - how many functions are used to compose the valence orbitals (by the number of letters) and how many GTOs are used for their representation (e.g. each of the *nlm* would have the value 1 for a s-function, the value 2 for a p-function,...). Examples are 3-21G, 6-31G for a Double Zeta basis set or 6-311G for a Triple Zeta basis set. If polarization functions are added, this is then denoted after the *G* with asterisks, e.g. 6-31G*.
One has to find the balance between increasing the basis set size and computation time with respect to accuracy. For the large polymers in this work, we choose to use only one polarization function because more polarization functions didn't affect the results for smaller molecules significantly and couldn't be computationally afforded for longer chains (see Sec. 3.5). In general, a small basis set yields almost the same results as a large basis set when a geometry optimization is performed. For excited state energies however, larger basis sets are usually more accurate up to a certain basis set size where an additional adding of more functions doesn't improve the results significantly. Yet, the accuracy of smaller basis sets (like 6-311G*) is still quite good in many cases[16],[74] - as long as polarization functions are used. In this work, all chain sizes were calculated with the same basis set that could be afforded for the longer chains (6-31G*).

2.8 Exchange and Correlation Errors

The description of exchange and correlations errors follows Ref.[1]. In the XC energy, the exchange energy is magnitudes larger than the correlation energy. Therefore the question

arises, why the exchange energy couldn't be calculated in HF theory, because there this part is exact whereas the 'difficult' correlation part could come from DFT. But this gives usually poor results, as the expressions for both parts are not identical which avoids essential error cancelations. The correlation energy is defined as the difference between the exact energy and the HF value. Exchange and correlation energy have a short- and a long-range part (in terms of the distance between electrons). However, the exchange functional in DFT is usually local and therefore short-ranged (they depend only on the density at a given point and the derivatives of the density). Therefore there is no error cancelation in the long-range regime.
A different treatment is the so called 'Generalized Kohn-Sham' approach which is described in the following.

2.9 Generalized Kohn-Sham Approach

This subsection follows the Review on "Tuned Range-Separated Hybrids in Density Functional Theory" by Baer, Livshits and Salzner.[10]
The Generalized Kohn Sham (GKS) approach is a method that leads to the same ground state density and energy as in the KS approach but the orbitals $\psi_\sigma(\mathbf{r}_i)$ and orbital energies $\epsilon_{i\sigma}$ are generally different. GKS uses Slater wavefunctions, but in contrast to the Hartree-Fock method GKS also includes correlation which leads in principle to the exact ground state density and energy of the many-body system.
In the GKS treatment, the Hamiltonian is not adjusted to a non-interacting and a real system - it keeps its usual form $H = T + V_{\text{ext}} + V_{\text{ee}}$ with $V_{\text{ext}} = \int v(\mathbf{r})\hat{n}(\mathbf{r})d^3r$ being the general potential energy of attraction to nucleus or other external potential fields, where $\hat{n}(\mathbf{r}) = \sum_{n=1}^{N} \delta(\mathbf{r} - \hat{\mathbf{r}}_n)$ is the electron density operator. The generalization of Eq. (15) is to break the minimum procedure into two parts[34]

$$E_{gs}[\eta, N] = \min_{\eta \to N} \left[\underbrace{\min_{\psi \to N} [\langle \psi | \, \hat{T} + \hat{V}_{ee} \, | \psi \rangle]}_{F[\eta]} + \int v(\mathbf{r})\eta(\mathbf{r})d^3r \right] \tag{30}$$

where $\psi \to \eta$ searches over all wavefunctions for which $\langle \psi | \, \hat{n}(\mathbf{r}) \, | \psi \rangle = \eta(\mathbf{r})$ and $\eta \to N$ runs over all positive density functions for which $\int \eta(\mathbf{r})d^3r = N$. The inner minimum $F[\eta]$ defines a universal density functional which is complicated and cannot be directly accessed. Similar to the HF approach, one part of the problem can be made accessible by performing

the minimum search only over limited N-electron Slater-determinants ϕ (denoted by S):

$$F_S[\eta] = \min_{\phi \to \eta}[\langle\phi|\,\hat{T} + \hat{V}_{\text{ee}}\,|\phi\rangle] \tag{31}$$

This leads to a direct definition of the correlation energy,[23]

$$E_C^{GKS}[\eta] = F[\eta] - F_S[\eta] \tag{32}$$

which inherits the whole electronic-structure problem and has to be approximated under DFT. Under several conditions (see Ref.[35]), Eq. (30) can be written as

$$E_{gs}[\eta, N] = \min_{\phi \to N}[\langle\phi|\,\hat{H}\,|\phi\rangle + E_C^{GKS}[\eta_\phi]], \tag{33}$$

where $\eta_\phi = \langle\phi|\,\hat{n}(\mathbf{r})\,|\phi\rangle$ corresponds to the electron density. The advantageous point of the GKS method is, that the minimizing Slater wavefunction $\widetilde{\phi}$ yields the same ground-state energy and the same density as the exact problem:

$$\left\langle\widetilde{\phi}\right|\hat{n}(\mathbf{r})\left|\widetilde{\phi}\right\rangle = \left\langle\widetilde{\psi}\right|\hat{n}(\mathbf{r})\left|\widetilde{\psi}\right\rangle. \tag{34}$$

Using N orthonormal orbitals $\phi_j(\mathbf{r})$ (j=1, ..., N) in the exchange part whose form is identical to the exchange part in HF theory

$$E_X^{GKS}[\{\phi_j\}] = -\frac{1}{2}\int\int \frac{|\sum_j \phi_j(\mathbf{r})\phi_j(\mathbf{r}')|^2}{|\mathbf{r}-\mathbf{r}'|} d^3r d^3r' \tag{35}$$

($E_X^{GKS}[\{\phi_j\}]$ denotes the functional of the sum of $\{\phi_j\}$), the XC orbital functional can be written as $E_{XC}^{GKS}[\{\phi_j\}] = E_X^{GKS}[\{\phi_j\}] + E_C^{GKS}[n_{\{\phi_j\}}]$, with $n_{\{\phi_j\}}(\mathbf{r}) = \sum_{j=1}^{N} |\phi_j(\mathbf{r})|^2$. In contrast to the XC energy of the KS approach in Eq. (19) which is a density functional, the GKS in an orbital functional. Another difference is that the exchange energy E_X^{GKS} is exact, so that the GKS approach needs only approximations for the correlation energy. The search for N normalized spin orbitals in Eq. (33) yields the GKS equations:

$$\left(-\frac{1}{2}\nabla^2 + v_{ext}(\mathbf{r}) + v_H(\mathbf{r})\right)\phi_j(\mathbf{r}) + \hat{K}_X\phi_j(\mathbf{r}) + v_C^{GKS}(\mathbf{r})\phi_j(\mathbf{r}) = \epsilon_j\phi_j(\mathbf{r}), \tag{36}$$

where

$$\hat{K}_X\phi_j(\mathbf{r}) = \frac{\delta E_X^{GKS}}{\delta\phi_j(\mathbf{r})} = -\sum_{k=1}^{N}\left[\phi_k(\mathbf{r})\int\frac{\phi_k(\mathbf{r}')\phi_j(\mathbf{r}')}{|\mathbf{r}-\mathbf{r}'|}dr'^3\right],\;\; v_C^{GKS}(\mathbf{r}) = \frac{\delta E_C^{GKS}}{\delta\eta(\mathbf{r})}, \tag{37}$$

and $v_H(\mathbf{r})$ is the Hartree potential. The form of the exchange operator $\hat{K}_X\phi_j(\mathbf{r})$ is identical to the form of $\hat{K}_{ij}$ in HF theory (see Eq. (7)) which are both non-local (depending both on $\mathbf{r}$ and $\mathbf{r}'$) - in contrast to the KS approach where only local potentials appear.

Similar to Koopman's Theorem for HF (see Sec. 2.3), there exists an Ionization Potential (IP) theorem for the GKS approach. It can be shown that in a system with N interacting electrons the following holds:[36],[37]

$$-\epsilon_{HOMO} = IP(N) \coloneqq E_{gs}(N-1) - E_{gs}(N). \tag{38}$$

In contrast to HF theory, where $-\epsilon_{HOMO}$ is not exactly the IP, in GKS the inclusion of the correlation energy allows Eq. (38) to hold exactly.

In the following, some of the most popular XC-functionals are presented. An important guide to construct approximate XC functionals is the asymptotic form ($r \to \infty$) of the potentials for finite systems.[10] It can be shown[36],[37] that to leading order in r^{-1}, the convergence behavior of the exact XC functional is

$$\begin{aligned}\text{KS}: v_X(\mathbf{r}) &\to -\frac{1}{r};\;\; v_c(\mathbf{r}) \to v_C^{\infty} - \frac{\mathbf{r}\cdot\alpha\cdot\mathbf{r}}{2r^6},\\ \text{GKS}: \hat{K}_X\phi_j(\mathbf{r}) &\to v_X(\mathbf{r})\phi_j(\mathbf{r});\;\; v_C^{GKS}(\mathbf{r}) \to v_C^{KS}(\mathbf{r}),\end{aligned} \tag{39}$$

where $v_l(\mathbf{r}) = \frac{\delta E_l^{KS}}{\delta\eta_l(\mathbf{r})}$, $l = H, X, C$, α is the polarizability tensor of the ionized system and v_C^{∞} is an arbitrary constant that can be taken as zero. The $1/r$ exchange behavior dominates the asymptotic form of the XC potential.

2.10 Approximate XC Functionals

In order to calculate DFT practically, approximations for the dependence of the XC functional on the densities must be used. There exist various sophisticated approximations.

- **The LDA (local density approximation)**

The LDA is the simplest approximation to the XC functional. It depends only on the density at the coordinate where the functional is evaluated $\eta_0 = \eta(\mathbf{r})$:[46]

$$E_{XC}^{LDA}[\eta] = \int d^3r \epsilon_{XC}^{HEG}[\eta_0 = \eta(\mathbf{r})], \tag{40}$$

where ϵ_{XC}^{HEG} is given by the energy per particle for the homogenous electron gas. Usually it is decomposed into a part referring to exchange and correlation:

$$\epsilon_{XC}^{HEG}[\eta(\mathbf{r})] = \epsilon_{X}^{HEG}[\eta(\mathbf{r})] + \epsilon_{C}^{HEG}[\eta(\mathbf{r})]. \tag{41}$$

The correlation part ϵ_C has to be approximated numerically due to the fact that only limiting expressions for the correlation density are known exactly. Various approaches, using different analytic forms for the correlation energy ϵ_C, have generated several LDA's for the correlation functional.
The XC potential $v_{XC}^{HEG} = \frac{d\epsilon_{XC}^{HEG}[\eta_0]}{d\eta_0}\Big|_{\eta_0=\eta(\mathbf{r})}$ is extremely short ranged as it only depends on the local density. Consequently the LDA potential decays exponentially with $r \to \infty$. This can be seen in the the exchange component of the homogenous electron gas which can be computed analytically[46]

$$v_X^{LDA}[\eta(\mathbf{r})] = -\frac{(3\pi^3)^{1/3}}{\pi} e^2 \eta^{1/3}(\mathbf{r}). \tag{42}$$

If the density drops of exponentially ($\eta(\mathbf{r}) \propto e^{-\alpha r}$) and the same happens with the exchange potential whereas the exact exchange part (Eq. 35) has the characteristic $-1/r$ behavior. This general problem of LDA and GGA's (discussed in the next subsection) is visualized in Fig. 2.

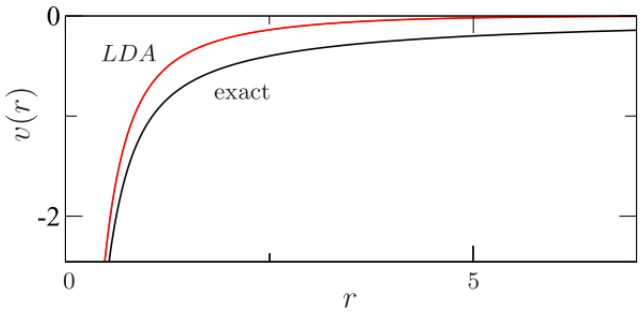

Figure 2: Exact and LDA KS potentials for the He atom. The exact potential decays like $-1/r$, whereas the LDA drops off exponentially. From Ref.[16]

This poor behavior far from the nuclei leads to poor eigenvalues for Rydberg states and some other inaccuracies.[16] This wrong long range behavior and its consequences also holds for the generalized gradient approximations.[10]
Despite these asymptotic problems and the large difference between the electronic density of the HEG and the confined density of atoms or molecules, LDA works astonishing well. Due to an error cancelation between the exchange and correlation part, the XC energy is generally underestimated by only 7%.[16]
However a significant limitation of LDA is 'overbinding' in solids: Lattice parameters are usually underestimated, whereas cohesive energies, phonon frequencies and elastic moduli are typically over-predicted.[48] This is improved by the next sophistication level - the generalized gradient approximation (GGA).

- **The Generalized Gradient Approximation (GGA)**
  The locally constant potential in the LDA is certainly not a good approximation for atoms or molecules, where large density gradients can appear. The GGA is an improvement, because it uses functionals that depend on the density and also on the gradient of the density:

$$E_{XC}^{GGA}[\eta_\alpha, \eta_\beta] = \int d^3r\, f(\eta_\alpha, \eta_\beta, \vec{\nabla}\eta_\alpha, \vec{\nabla}\eta_\beta) \tag{43}$$

  As well as in the LDA, E_{XC}^{GGA} can be decomposed into an exchange and a correlation part. The exchange part reads[47]

$$E_X^{GGA} = E_X^{LDA} - \sum_\sigma \int d^3r\, F(S_\sigma)\, \eta_\sigma^{4/3}(\mathbf{r}) \tag{44}$$

  where σ runs over α and β spins and the reduced density gradient is

$$S_\sigma = \frac{|\vec{\nabla}\eta_\sigma(\mathbf{r})|}{\eta_\sigma^{4/3}(\mathbf{r})}. \tag{45}$$

  There are many different functionals which differ in this function $F(S)$ - mostly by the way they are constructed: Some take known exact conditions into account (e.g. size consistency or scaling relations), whereas others fix free parameters by empirical values.
  In principle one can combine every exchange functional with every correlation functional. The most popular functionals using this approximation without empirical pa-

rameters are BLYP (B88[26] for exchange and LYP[27] for correlation) and PBE.[31],[32] The total energies of LDA are generally improved by a factor of 2-5.[16] Additionally the overbinding tendency of LDA is reduced, e.g. the hydrogen bonds are better but they still don't obey chemical accuracy of an average error of $\sim$ 1 kcal/mol.[47],[49]

- **Hybrid Functionals**
  Hybrid functionals are mixtures of the Hartree-Fock and the DFT exchange potential. The mixing is motivated by improved results of some properties like the HOMO-LUMO gap. The correlation energy is much smaller than the exchange energy and Hartree-Fock theory evaluates the exchange energy exactly. This gives another argument for the combination of HF exchange with a correlation functional of DFT. In order to preserve the error cancellation of GGA's, only a small portion of exact exchange (20%-25%) is mixed in. The general form of mixing a percentage c_{HF} of HF exchange into an GGA is:

$$E_{XC} = E_C + (1 - c_{HF})E_{X,\text{local}} + c_{HF}E_{X,HF} \tag{46}$$

  where $E_{X,\text{local}}$ denotes the local DFT exchange energy (see Eq. (41) and Eq. (44)), and $E_{X,HF}$ the HF exchange energy (third term in Eq. (7)). The most popular hybrid functional is 'B3LYP' (Becke,[26] three-parameter, Lee-Yang-Parr[27]),[28] which merges the exchange-correlation functionals BLYP from the GGA and the LDA with the Hartree-Fock exchange part by use of three empirical parameters a_0, a_x and a_c:

$$E_{XC}^{B3LYP} = E_{XC}^{LDA} + a_0(E_X^{HF} - E_X^{LDA}) + a_x(E_X^{GGA} - E_X^{LDA}) + a_c(E_C^{GGA} - E_C^{LDA}). \tag{47}$$

  Another hybrid functional is e.g. PBE0,[30] where 25% of HF exchange is mixed into the PBE functional. These inclusions of HF exchange often improve calculated results and make hybrids the most common form of used functionals.
  The structural properties like bondings lengths, lattice constants or bulk moduli of molecular systems are improved with respect to PBE. Electronic properties like band gaps are usually underestimated by PBE in extended systems.[50] A mixture of HF tends to widen the gap (although they are often still somewhat underestimated[74],[75]). However, the optimal fraction of HF exchange depends on the specific properties of interest - the most convenient choices for the investigated polymers in this work are discussed in Sec. 3.5.
  Yet, hybrids are no all-round solution as they lack e.g. in the description of metallic

systems and charge-transfer states.[42] Therefore the improvement of so-called long-range-corrected (LRC) XC functionals is described in the next section as it yields promising results in many cases.

2.11 Long-Range-Corrected DFT

A cure to the wrong long-range behavior of LDA and other semilocal XC functionals is to use long-range-corrected (LRC) XC functionals.[38],[39] The main idea is the use of range-separated functionals that partition the Coulomb operator into a short-range and long-range component, ruled by the parameter γ - e.g. by utilizing the standard error-function erf(x):[11]

$$\frac{1}{r} = \frac{1 - \mathrm{erf}(\gamma r)}{r} + \frac{\mathrm{erf}(\gamma r)}{r}. \tag{48}$$

The first term is a Coulomb operator decaying to zero on a length scale of $\approx 1/\gamma$ and is therefore short-ranged (SR). The second term dominates at large r accounting for the long-range (LR) behavior. Starting from the hybrid exchange energy in Eq. (46), the partitioned 'range-separated' Coulomb operator transforms the exchange energy to

$$E_{XC}^{LRC} = E_C + (1 - c_{HF})E_{x,\mathrm{local}}^{SR} + c_{HF}E_{X,HF}^{SR} + E_{X,HF}^{LR} \tag{49}$$

where $E_{X,HF}^{SR}$ and $E_{X,HF}^{LR}$ is the γ-separated HF exchange energy using short - and long-range components of the Coulomb operator and the local DFT exchange energy $E_{x,\mathrm{local}}^{SR}$ is evaluated using the short-range part while the correlation energy E_c is not modified.
Semilocal DFT functionals only approximate the exchange part, whereas in HF this part is exact. The vital point is that the exact HF exchange improves the error cancellation. The coulomb term J_{ii} and HF exchange term K_{ii} in Eq. (6) cancel each other and prohibit therefore self-interaction.
Without the inclusion of HF (in semilocal DFT like LDA), spectacular failures' appear due to delocalization errors caused by the missing error cancellation.[15] These errors are avoided by including exact exchange - however for hybrid functions this advantage is only used partially because only a fraction of HF exchange is mixed in (e.g. 20% in B3LYP). In contrast LRC XC functionals allow 100% HF exchange in the long range regime and therefore 100% exchange-correlation error cancellation what improves the results systematically. The only critical point in LRC XC functionals is the system specific choice of the range-separation parameter γ.
The long-range-corrected DFT can be applied to semilocal and hybrid XC functionals.

Long range corrections of semilocal XC functionals are called range separated hybrids (RSH's). The quality of these corrections depends on the choice of the range-separation parameter γ which is highly system dependent. The tuning of this parameter is discussed in the next section.

2.12 Tuning of the Range-Separation Parameter γ

This subsection follows the Review on "Tuned Range-Separated Hybrids in Density Functional Theory" by Baer, Livshits and Salzner.[10]

It can be shown that the γ parameter of range-separated hybrids (RSH's) depends significantly on the density. As in turn the energies depend strongly on the density, the need for an optimization of the γ parameter becomes obvious. Due to the system dependent density, the pre-tuning of γ for each considered system yields much better results than the use of a standard fixed parameter for all systems.

The IP theorem (Eq. 38) is usually violated by conventional DFT functionals as e.g. the B3LYP HOMO energy is only 70% of the experimental IPs for an assortment of small molecules as shown in Fig. 3. The Bear-Neuhauser-Livshits-RSH BNL* XC functional however, which uses an system dependent ab-initio-motivated tuned range parameter γ (the asterisk indicates parameter tuning), is obviously system dependent and shows only an absolute deviance of $\approx 5\%$.

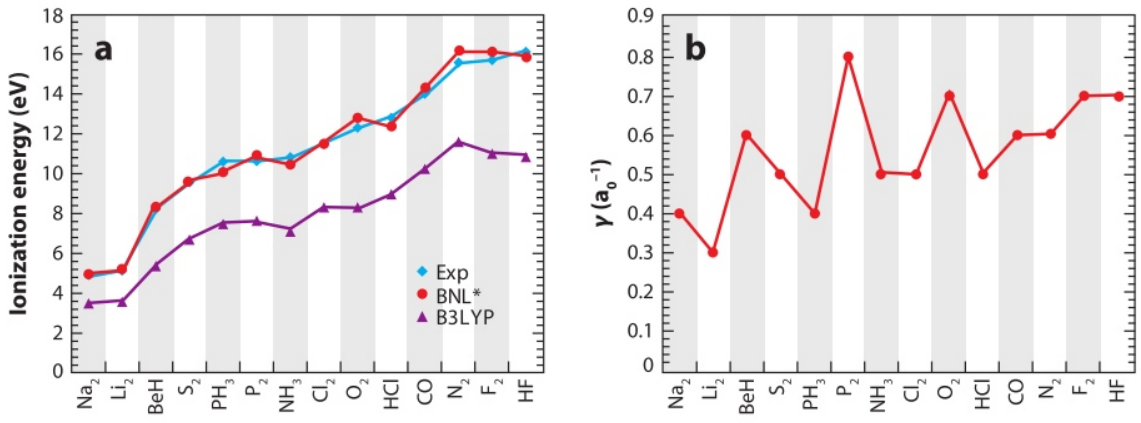

Figure 3: (a) The experimental vertical ionization energies versus calculated ionization potentials for the B3LYP and BNL* XC functional for an assortment of small molecules with basis set cc-pVTZ. Exp. data from Ref.[33] (b) The values of the tuned range parameter γ used for the BNL* calculation. Both graphs from Ref[10]

The tuning of the γ parameter, is essentially to minimize the following error function[62]

$$\Delta_{IP}(\gamma) = |\epsilon^{\gamma}_{HOMO} - (E^{\gamma}_{GS}(N) - E^{\gamma}_{GS}(N-1))|, \tag{50}$$

where the superscript γ indicates that the Coulomb operator in the included XC functionals is γ-dependent partitioned as introduced in Eq. (48). The total energy of the HOMO ϵ_{HOMO} should be equal to the ionization energy gained by subtraction the total energies of the N electron and N-1 electron system in the ground state E_{GS}. The γ value, where this difference is minimal yields the optimal long-range parameter for the system.
This tuning procedure was applied to all molecules considered in this work and compared with the standard XC functionals B3LYP and PBE.

2.13 Time Dependent Density Functional Theory

This subsections follows mainly the TDDFT Review by Elliott et. al[16] and the TDDFT Lecture Notes of Gross and Burke.[17] The Time Dependent Density Functional Theory (TDDFT) can describe the behavior of electrons, for example when a time-dependent perturbation like a laser field is applied.
The focus of this work is on electronic transitions of molecular systems. So why can't DFT describe electronic transitions? In principle each ground state calculation could yield the exact eigenvalues which are the transition energies of a molecular system. However ground state DFT is based on the variational principle which can only describe the electronic density of the ground state. Using time dependent perturbation theory is a method to bypass this problem - even due to the fact that it is still based on the ground state results. It yields corrections to the ground state density and therefore to the pure ground state KS excitation energies.
Generally the DFT applications can be grouped in three categories: nonperturbative regimes, linear (and higher-order) response and ground state applications. Beyond linear-response theory, what is the focus of this work, TDDFT also works for challenging non-perturbative applications.[43]
The basis of TDDFT is a analog statement to the Hohenberg-Kohm theorem for DFT - the Runge-Gross theorem.[44] It states that there is a one-to-one mapping between time-dependent one-body densities $\rho(\mathbf{r}, t)$ and time-dependent one-body potentials $v_{\text{ext}}(\mathbf{r}, t)$, for a given initial state Ψ_0. That means, that the time-dependent potential can be expressed

as a functional of the time dependent density (and the initial state):

$$v_{\text{ext}}[\eta; \Psi_0](\mathbf{r}, t). \tag{51}$$

This functional is due to the time dependency much more complex than in the ground state case.[16] There exists a spin-dependent generalization, leading to $v_{\text{ext}}(\mathbf{r}, t)$ being a functional of the spin densities η_α, η_β.[45]
Analogous to ground state DFT, the next step is to define a fictitious system of noninteracting electrons satisfying the time-dependent Kohn-Sham equations

$$i\frac{\partial \phi_{j\sigma}(\mathbf{r}, t)}{\partial t} = \left[-\frac{\nabla^2}{2} + v_{KS}[\eta](\mathbf{r}, t)\right] \phi_{j\sigma}(\mathbf{r}, t) \tag{52}$$

where the potential is determined, such that it gives (due to the RG theorem) the spin densities of the real interacting system:

$$\eta_\sigma(\mathbf{r}, t) = \sum_{j=1}^{N} |\phi_{j\sigma}(\mathbf{r}, t)|^2. \tag{53}$$

The exchange-correlation potential is then defined in the KS-potential

$$v_{KS}(\mathbf{r}, t) = v_{\text{ext}}(\mathbf{r}, t) + \int d^3r' \frac{\eta(\mathbf{r}', t)}{|\mathbf{r} - \mathbf{r}'|} + v_{XC}(\mathbf{r}, t), \tag{54}$$

where the term in the middle is the usual Hartree potential, but for a time-dependent density. If both the interacting ϕ_0 and the KS initial wavefunctions Φ_0 are nondegenerate ground states, the exchange-correlation potential is only a functional of the time-dependent density.
The most common application is the weak perturbation regime which describes typical spectroscopic experiments well. For perturbed systems only the potential in the vicinity of the initial state needs to be known, leading to small changes in density with time. Therefore in linear response, only densities close to the initial state need to be taken into account, where the ground state is taken to be non-degenerate

$$\eta(\mathbf{r}, t) = \eta_{GS}(\mathbf{r}) + \delta\eta(\mathbf{r}, t), \tag{55}$$

leading to

$$v_{XC}[\eta_{GS}+\delta\eta](\mathbf{r},t) = v_{XC}(\mathbf{r}) + \int dt' \int d^3r' f_{XC}[\eta_{GS}](\mathbf{r},\mathbf{r}',t-t')\delta\eta(\mathbf{r}',t'), \tag{56}$$

where f_{XC} is the exchange-correlation kernel evaluated at the ground-state density:

$$f_{XC}[\eta_{GS}](\mathbf{r},\mathbf{r}',t-t') = \left.\frac{\delta v_{XC}(\mathbf{r},t)}{\delta\eta(\mathbf{r}',t')}\right|_{\eta=\eta_{GS}}. \tag{57}$$

This XC-kernel is complex but still much more manageable then the full time-dependent XC potential, because it is a functional of the ground-state density alone. Linear response in f_{XC} is characterized in the point-wise susceptibility $\chi[\eta_{GS}](\mathbf{r},\mathbf{r}',t-t')$ because it defines the response of the ground state density to a small change in the external potential

$$\delta\eta(\mathbf{r},t) = \int dt' \int d^3r' \chi[\eta_{GS}](\mathbf{r},\mathbf{r}',t-t')\delta v_{ext}(\mathbf{r}',t') \tag{58}$$

where χ tells how the density will change at a point $\mathbf{r}$ and time t if the external potential at point $\mathbf{r}'$ and time t' is changed slightly. The analog ground-state KS System is denoted by χ_{KS}, describing how noninteracting KS electrons would respond to δv_{KS} (where v_{KS} is defined in Eq. (54)). The interacting and noninteracting case must yield the same density response according to the Runge-Gross theorem:

$$\delta\eta(\mathbf{r},t) = \int dt' \int d^3r' \chi_{KS}[\eta_{GS}](\mathbf{r},\mathbf{r}',t-t')\{\underbrace{\delta v_{ext}(\mathbf{r}',t') + \delta v_H(\mathbf{r}',t') + \delta v_{XC}(\mathbf{r}',t')}_{\delta v_{KS}}\}. \tag{59}$$

Comparing this density change with the change of the interacting system (58) and using Eq. (54), the TDDFT linear response equation in frequency space may be written as

$$\chi(\mathbf{r},\mathbf{r}',\omega) = \chi_{KS}(\mathbf{r},\mathbf{r}',\omega) + \int d^3r_1 \int d^3r_2 \chi_{KS}(\mathbf{r},\mathbf{r}_1,\omega) \underbrace{\left\{\frac{1}{|\mathbf{r}_1-\mathbf{r}_2|} + f_{XC}(\mathbf{r}_1,\mathbf{r}_2,\omega)\right\}}_{:=f_{HXC}} \chi(\mathbf{r}_2,\mathbf{r}',\omega), \tag{60}$$

where all ingredients are functionals evaluated at the ground state density and f_{HXC} is called the Hartree XC kernel. This equation is the key to electronic excitations via TDDFT. The poles of χ_{KS} are at the single-particle excitations of the KS system

$$\chi_{KS}(\mathbf{r},\mathbf{r}',\omega) = 2\lim_{\epsilon\to 0^+}\sum_q \left\{\frac{\xi_q(\mathbf{r})\xi_q^*(\mathbf{r}')}{\omega-\omega_q+i\epsilon} - \frac{\xi_q^*(\mathbf{r})\xi_q(\mathbf{r}')}{\omega-\omega_q-i\epsilon}\right\}, \tag{61}$$

where q is a double index for the transition from an occupied KS orbital i to an unoccupied KS orbital a, $\omega_q = \epsilon_a - \epsilon_i$ and $\xi_q(\mathbf{r}) = \phi_i^*(\mathbf{r})\phi_a(\mathbf{r})$ where ϵ_i is the eigenenergy of the KS state ϕ_i.
Otherwise, the kernel in Eq. (60) leads to corrections for the transitions from the KS values to the 'true' values, although the response of the ground-state KS part usually stays dominant. Furthermore, the strength of the poles in Eq. (61) can be related to the intensities of the optical transition (oscillator strength).[55], [58]
The standard approach in quantum chemistry to extract the excitations from TDDFT is Casida's method[55] to convert the search for poles of the response functions into a large eigenvalue problem within the space of the single-particle excitations of the system.[59], [60] For frequency-independent kernels, the poles of χ can be found by solving the Casida eigenvalue equation,[56], [57] which is often denoted in this form:

$$\begin{pmatrix} A & B \\ B^* & A^* \end{pmatrix} \begin{pmatrix} \mathbf{X} \\ \mathbf{Y} \end{pmatrix} = \omega \begin{pmatrix} 1 & 0 \\ 0 & -1 \end{pmatrix} \begin{pmatrix} \mathbf{X} \\ \mathbf{Y} \end{pmatrix}. \tag{62}$$

In this representation $(\mathbf{X}, \mathbf{Y})$ its the amplitude eigenvector and the matrix elements in the KS basis are (following Ref.[51] and[52])

$$A_{ai\sigma,bj\tau} = \delta_{\sigma\tau}\delta_{ij}\delta_{ab}(\epsilon_{a\sigma} - \epsilon_{i\sigma}) + (ai\sigma|jb\tau) + (ai\sigma|f_{XC}|jb\tau) \tag{63}$$

where σ and τ are the spin indices at $\mathbf{r}$ and $\mathbf{r}'$ and

$$B_{ai\sigma,bj\tau} = (ai\sigma|bj\tau) + (ai\sigma|f_{XC}|bj\tau) \tag{64}$$

where the two-electron integrals are written in Mulliken notation

$$(ai\sigma|jb\tau) = \int\int d\mathbf{r}d\mathbf{r}'\phi_{a,\sigma}^*(\mathbf{r})\phi_{i,\tau}^*(\mathbf{r}')g(\mathbf{r},\mathbf{r}')\phi_{j,\sigma}(\mathbf{r})\phi_{b,\sigma}(\mathbf{r}') \tag{65}$$

(labels i,j,... are used for occupied, a,b,... for unoccupied orbitals) and the operator $g(\mathbf{r},\mathbf{r}') = |\mathbf{r} - \mathbf{r}'|^{-1}$. Casida's TDDFT matrix equation is the linear response expression that can be solved self-consistently. An unitary transformation yields the hermitian matrix for the TDDFT excitation energies[56] $\Omega = (\mathbf{A} - \mathbf{B})^{1/2}(\mathbf{A} + \mathbf{B})(\mathbf{A} - \mathbf{B})^{1/2}$ with matrix elements

$$\Omega_{ai\sigma,bj\tau} = \delta_{\sigma\tau}\delta_{ij}\delta_{ab}\omega_{ai\sigma}^2 + 2\sqrt{\lambda_{ai\sigma}\omega_{ai\sigma}}K_{ai\sigma,bj\tau}\sqrt{\lambda_{bj\tau}\omega_{bj\tau}}, \tag{66}$$

where the differences of the KS eigenvalues are $\omega_{ai\sigma} = \epsilon_{a\sigma} - \epsilon_{i\sigma}$ and $\lambda_{ai\sigma} = n_{a\sigma} - n_{i\sigma}$ are

the differences between the occupation numbers. The coupling matrix $\hat{K}$ is given in the adiabatic approximation (described below) as:

$$\begin{gathered} K_{ai\sigma,bj\tau} = (ai\sigma|jb\tau) + (ai\sigma|f_{XC}|jb\tau) = \\ \int d^3r \int d^3r' \phi^*_{a,\sigma}(\mathbf{r})\phi^*_{i,\tau}(\mathbf{r}') \left(g(\mathbf{r},\mathbf{r}') + f_{XC}(\mathbf{r},\mathbf{r}')\right) \phi_{j,\sigma}(\mathbf{r})\phi_{b,\tau}(\mathbf{r}'). \end{gathered} \tag{67}$$

The oscillator strengths f_n, can be expressed as[55]

$$f_n = \frac{2}{3} \sum_{\alpha=\{x,y,z\}} |D_\alpha \hat{S}^{1/2} F_n|^2 \tag{68}$$

where F_n are the eigenvectors of $\mathbf{\Omega} F_n = \omega_n^2 F_n$, $S_{ai\sigma,bj\tau} = \delta_{\sigma\tau}\delta_{ij}\delta_{ab}\lambda_{ai\sigma}\omega_{bj\tau}$ and the dipole matrix elements are $D_{\alpha,ai\sigma} = \int d^3r \phi^*_{a,\sigma}(\mathbf{r})\alpha\phi_{i,\sigma}(\mathbf{r})$.
Similar to the ground state case, the practical TDDFT calculations require approximations for the unknown XC potential. The most common approximation is the 'adiabatic approximation' from which one deduces that for a slowly varying density $\eta(t)$, the effective potential is the instantaneous ground state potential[16]

$$v^{adia}_{XC}[\eta](\mathbf{r}t) = v^{GS}_{XC}[\eta_0](\mathbf{r})\Big|_{\eta_0(\mathbf{r})=\eta(\mathbf{r}t)}. \tag{69}$$

The adiabatic approach is used even when the density changes rapidly because numerical[40] and theoretical[41] studies indicate that it can be reliable even for strongly non-adiabatic situations. From the form of the adiabatic approximation it is obvious that any ground state approximation (LDA, GGA, hybrid) provides automatically an adiabatic approximation for TDDFT which can be used in practical applications.
In principle linear response calculations can be divided in two parts[16] where both parts use approximations leading to built-in errors:

- The ground state DFT calculation provides zero-order approximations to the optical transitions
- The TDDFT linear response calculation is based on the orbitals of the ground state calculation which corrects the transitions into the optical transitions of the real system.

2.14 Asymptotic Scaling of TDDFT Matrix Elements

In order to analyze the dependence of the excitation energies on the system size, three types of two-electron integrals appearing in TDDFT have to be analyzed - the Coulomb integral, the semilocal DFT XC kernel and the exact HF exchange term (if hybrids/LRC XC functionals are used). The asymptotic scaling of these with the system size was analyzed by Scuseria et. al.[51] In order to simplify the expression for the TDDFT excitation energy, the Tamm-Dancoff approximation (TDA)[82] is used by setting $\mathbf{B} = 0$ in Eq. (62) (which doesn't change the result of the full TDDFT system regarding asymptotic behavior). With this, Casida's eigenvalue equation reduces to:

$$\mathbf{AX} = \omega\mathbf{X} \tag{70}$$

with $\mathbf{A}$ defined as before:

$$A_{ai\sigma,bj\tau} = \delta_{\sigma\tau}\delta_{ij}\delta_{ab}(\epsilon_{a\sigma} - \epsilon_{i\sigma}) + (ai\sigma|jb\tau) + (ai\sigma|f_{XC}|jb\tau). \tag{71}$$

The first term is the pure KS gap, the second term the Coulomb integral and the third term the semilocal integral with the TDDFT XC kernel (defined in Eq. (57)) which is used in LDA and all GGA XC functionals.
For hybrids the matrix elements of $\mathbf{A}$ are modified as follows:

$$A_{ai\sigma,bj\tau} = \delta_{\sigma\tau}\delta_{ij}\delta_{ab}(\epsilon_{a\sigma} - \epsilon_{i\tau}) + (ai\sigma|jb\tau) + c_{HF}(ab\sigma|ij\tau) + (1 - c_{HF})(ai\sigma|f_{XC}|jb\tau). \tag{72}$$

Scuseria et. al[51] examines the system dependent scaling of the appearing two-electron integrals with the number N of unit cells for a periodic system depending on the dimensionality - here we concentrate on 3D systems.
The Colomb integral in Eq. (72) originates from the Hartree exchange part in the potential. This exchange is a non-local matrix overlap and is therefore always smaller than the full Coulomb interaction ($\propto 1/r$) - it scales like $\log r^3/r^3$. The third term is the HF exchange term which takes in the adiabatic approximation the form of the atomic centered Coulomb integral and scales therefore like $1/r$. The last term denotes the semilocal DFT exchange-correlation kernel integrals which decay due to incomplete error cancellation too fast like $1/r^3$ as shown in Fig. 4.
Consequently, if no HF exchange term is included, the matrix elements scale like $\log r^3/r^3 + 1/r^3$ what permits a correct long range behavior compared to $1/r$. Inclusion of exact HF

exchange is therefore vital.

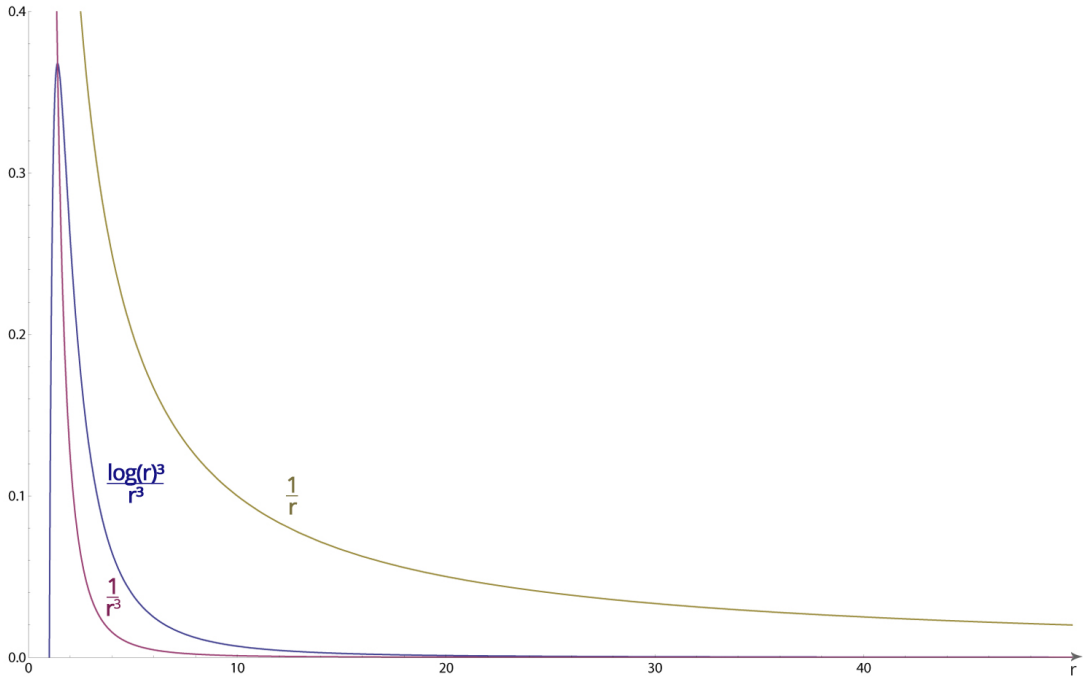

Figure 4: Instead of the $1/r$ scaling, the matrix elements for Coulomb drop off much too fast like $\log r^3/r^3$ as well as the semilocal DFT exchange-correlaction element scales like $1/r^3$. The inclusion of the Hartree exchange term adds the correct $1/r$ scaling which is important to describe the correct long range behavior.

The asymptotic behavior of the excitation energies can now be used to estimate the system size dependence of the oscillator strength as shown in the next section.

2.15 Particle-in-a-Box Model and Oscillator Strengths

As electrons/holes in π-conjugated polymers are delocalized along the chain direction, some basic properties can be deduced from the simple particle-in-a-box model which confines an electron in a certain space.
One observation is that the excitations energies decrease with the chain length. This is due to the known energy relation (in atomic units)

$$E_n(L) = \frac{n^2\pi^2}{2L^2} \tag{73}$$

where L is the length of the box and $n \in \mathbb{Z}^+$, leading to this expression for the transition energy:

$$\Delta E_{n\to n+1}(L) = \frac{\pi^2}{2L^2}(2n+1). \tag{74}$$

The excitation energy scales like $1/L^2$ with the box length L. This is an estimation of the behavior of the pure KS excitation energy $\epsilon_a - \epsilon_i$. In order to estimate the scaling of the oscillator strength we first need the wavefunction of a particle in a potential well, whose potential is defined as

$$V(x) = \begin{cases} 0, & 0 \le x \le L, \\ \infty, & \text{otherwise.} \end{cases} \tag{75}$$

The wavefunction solving the stationary Schrödinger equation for the system is:

$$\psi_n(x) = \begin{cases} \sqrt{\frac{2}{L}}\sin(\frac{n\pi x}{L}), & 0 \le x \le L, \\ 0, & \text{otherwise.} \end{cases} \tag{76}$$

The general expression of the oscillator strength f is related to the transition energy $\Delta E_{n\to n+1}$ (where the length dependence enters) and the transition dipole matrix element $D_{n\to n+1}$:[63]

$$f = \frac{8\pi^2 \Delta E_{n\to n+1}}{3}|D_{n\to n+1}|^2 = \frac{4\pi^4(2n+1)}{3L^2}|D_{n\to n+1}|^2 \tag{77}$$

with

$$D_{n\to n+1} = \int \psi_n x \psi_{n+1} dx = -\frac{8Ln(1+n)}{\pi^2(2n+1)^2}. \tag{78}$$

By inserting this in Eq. (77), we get

$$f = \frac{4\pi^4(2n+1)}{3L^2}|D_{n\to n+1}|^2 = \frac{4\pi^4(2n+1)}{3L^2} \cdot \left\{\frac{8Ln(1+n)}{\pi^2(2n+1)^2}\right\}^2 = \frac{16^2 n^2(1+n)^2}{3(2n+1)^3} \tag{79}$$

where the length dependence drops out.

Assuming that the L^2 length dependence of the dipole matrix element D^2 holds also in TDDFT, would roughly give the behavior of the scaling of the oscillator strength. For semilocal XC functionals (with $E^{TDDFT} \sim \alpha/L^2$) the length dependence would drop out, leading to a constant f. In contrast, XC functionals with a fraction of HF exchange ($E^{TDDFT} \sim \alpha/L^2 + \beta/L$) would show a linear scaling of f with L.

This behavior is observed by Tretiak et al.[94] - only functionals including HF fraction like B3LYP or LRC XC functionals yield an oscillator strength that scales linearly with the

chain length. In this work this linear scaling is also confirmed (see Sec. 3.9).
Of course the combination of the particle-in-a-box oscillator strength and the TDDFT asymptotic behavior of the excitation energy is a very rough approximation, as the oscillator strength of the I-th excited state in TDDFT is more complex than the simple one-particle oscillator strength (see Eq. 68).
The difference to the one-particle system are the non-diagonal elements originating from the eigenvector F_n, contributing to a mixture of different states for one transition. The Thomas-Reiche-Kuhn sum rule[90]–[92] holds for the TDDFT oscillator strengths,[93] because they are in principle exact

$$\sum_I f_I = N, \tag{80}$$

where N is the number of electrons in the system. From this relation it seems logical that the oscillator strength for the same excited state I - which has to be between $0 \leq f_I \leq N$ - scales linearly with the number of electrons N corresponding to the length of the system.

3 Methodology and Results

The subject of this master thesis is related to the experiment of the group of Lupton,[9] which is introduced in detail in the next subsection. The simplified polymer geometry used for all kind of calculations is introduced in Sec 3.2. Next, the motivation behind using naturally twisted or forced planar structures is discussed (Sec. 3.3). After describing the computational details used in the calculations (Sec. 3.4), the performance of the used functionals in the context of this work is pre-judged in Sec. 3.5. Special attention is paid then to the energetic ordering of the two lowest singlet excited states, as they are known to be sorted sometimes wrongly. Our indications on whether these states in the current case can be trusted are explained in Sec. 3.6. The different excitation energies that can be gained with TDDFT are explained next (Sec. 3.7). Afterwards, the scaling of the LRC parameter with the polymer lengths is compared to expectations (Sec. 3.8). In Sec. 3.9 the results from absorption energies are shown followed by the general results for transition energies in the context of the experiment (Sec. 3.10). Finally the localization behavior in the first excited triplet state is shown and compared to the suggestions of the group of Lupton in Sec. 3.11. Reasons for deviances to experiment are given in the last section 3.12. Tables for all kind of exception energies can be found in the appendix 5.

3.1 Input from the Experiment

In 2010, the group of Lupton[9] investigated the singlet-triplet (S-T) splitting in π-conjugated phosphorescent polymers and showed that the S-T gap can be tuned by choosing different types of triphenylene based polymers. These polymers show in contrast to most conjugated hydrocarbons a phosphorescence at low temperatures.

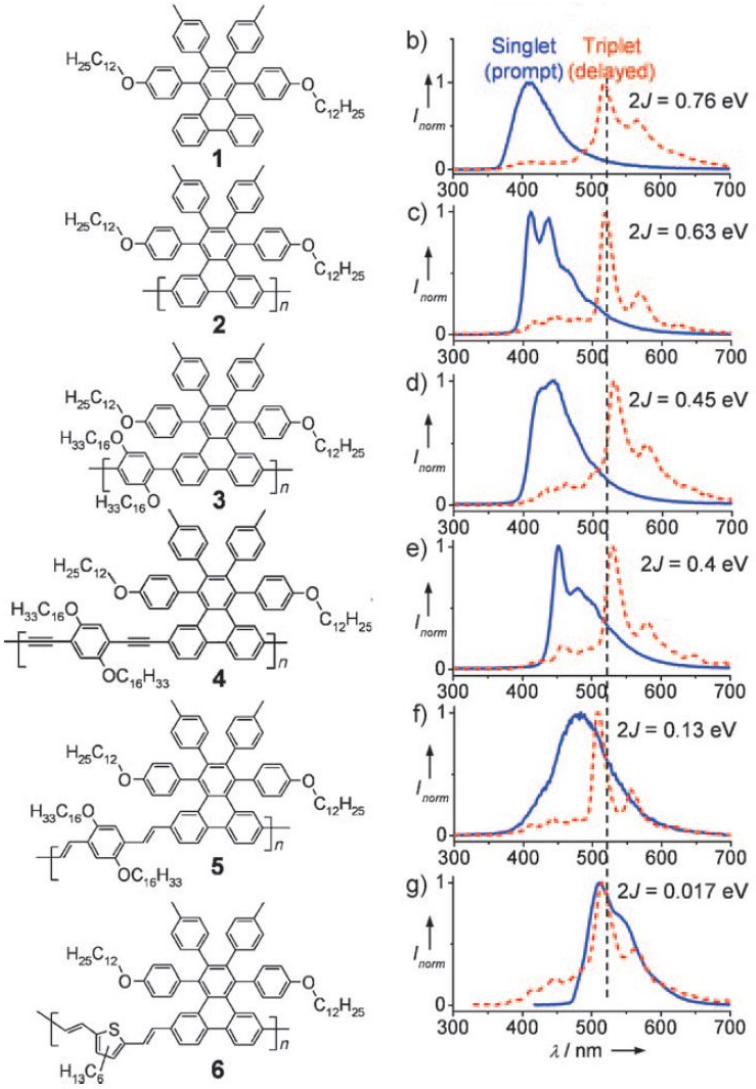

Figure 5: Fluorescence (prompt emission) and phosphorescence (delayed emission) from a triphenylene-based monomer and conjugated copolymers, dispersed in a polystyrene matrix at 25 K. a) Delocalization of singlet excitations (blue) with triplets (red) localized at the triphenylene unit. b)–g) Singlet (solid blue line, integrated 0-2 ns after excitation) and triplet (dashed red line) spectra of the monomer **1** (0.1–1.1 ms delay after excitation), the homopolymer **2** (9–10 ms delay), the para-phenylene copolymer **3** (1–2 ms delay), the ethynylene copolymer **4** (1.5–2.5 ms delay), phenylene vinylene copolymer **5** (0.02–1.02 ms delay), and the thienylene vinylene copolymer **6** (0.05– 5.05 ms delay). The exchange splitting 2J is estimated from the peak separations. The dashed black line indicates the average triplet peak position. From Ref.[9]

Different polymer materials were dispersed at a 1% weight ratio in polystyrene at 25 K. The group observed that the incorporation of the triphenylene based monomer **1** as depicted

in Fig. 5 into the polymer backbone led to a fully conjugated π system, where the triplet state seems to be localized on the triphenylene unit whereas the singlet state is delocalized over multiple repeat units.

Prompt luminescence (detected within 2 ns coinciding with the laser pulse) is caused by fluorescence from the singlet state whereas the delayed phosphorescence originates from the triplet state.[65] The copolymers show all a similar triplet spectrum at the same energetic position (the average peak position is marked with a dashed line in Fig. 5), whereas the energy of the singlet peak strongly depends on the details of the polymer backbone.[66] An accurate measurement of the magnitude of exchange interaction (2J) is provided by the energetic shift between fluorescence and phosphorescence.[64] The fact that the singlet emission shifts towards the triplet emission from monomer **1** to polymer **6**, whereas the triplet level remains almost unchanged, implies that singlet and triplet excitations can form on different parts of the conjugated system.[67] This indicates that the splitting could be tuned or that even the regular level ordering of singlet and triplet could be inversed.[9]

As the TDDFT calculations for chains with more than 260 atoms were for some XC functionals computationally too time intense, the number of basic units in a chain was limited to n=6.

In order to compare the results with experiment, it is important to estimate how many basic units one polymer chain in the experiment contains. This can be roughly estimated from the supporting information of the mass spectra provided by Lupton et. al.[9]

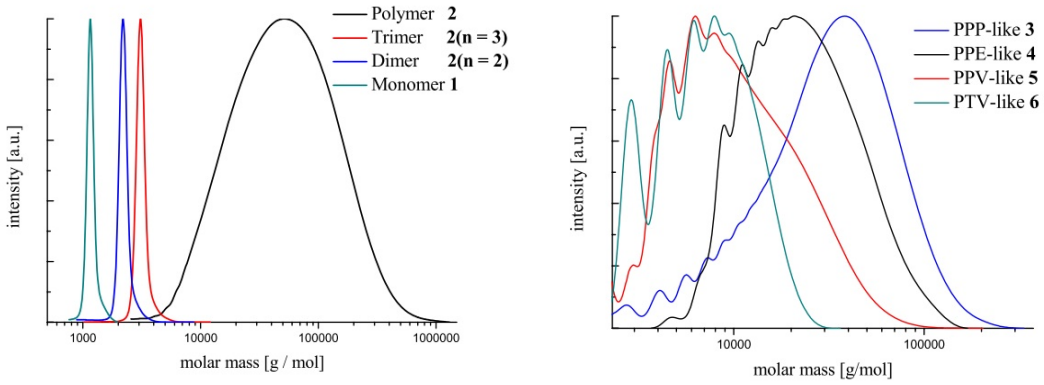

Figure 6: Mass spectrum for the monomer and polymers used in the experiment of Lupton[9]

Estimations from Fig. 6 yield the number of basic units in each polymer: approximately 48-52 units for the triphenylene polymer **2**, around 32-34 units for polymer **3**, 15-17 units for polymer **4** and only 5-7 units for polymer **5** and 4-6 units for polymer **6**. Therefore the

TDDFT results for polymer **5** and **6** can be directly compared (and of course the result for monomer **1**), whereas the other polymer types **2**, **3**, and **4** can't be calculated up to comparable length scales. However the corresponding trends for the excitation energies and triplet localizations give also reasonable results.

3.2 Simplified Polymers

In order to set up the main chemical units for the simulations as depicted in Fig. 5, we first used pure triphenylene to build a chain - neglecting the functional groups for all polymers but the monomer. We modify the polymer numbering of Lupton et. al slightly and denote a n time unit repetition e.g. as $P2_n$ where $P2$ stands for polymer **2**, except the monomer $M1$, which is a triphenylene monomer as it includes only one repetition unit. The monomer geometry was built by including the functional groups and the two oxygen atoms but neglecting the alkane tail (simplified geometry is depicted in Fig. 7). Additionally to the pure triphenylene polymer **2**, a PPP-like copolymer **3**, a PPE-like copolymer **4**, a PPV-like copolymer **5** and a PTV-like copolymer **6** served as basic units for polymers with length n. The geometries of the basic units that were used in all calculations are shown in the following figure.

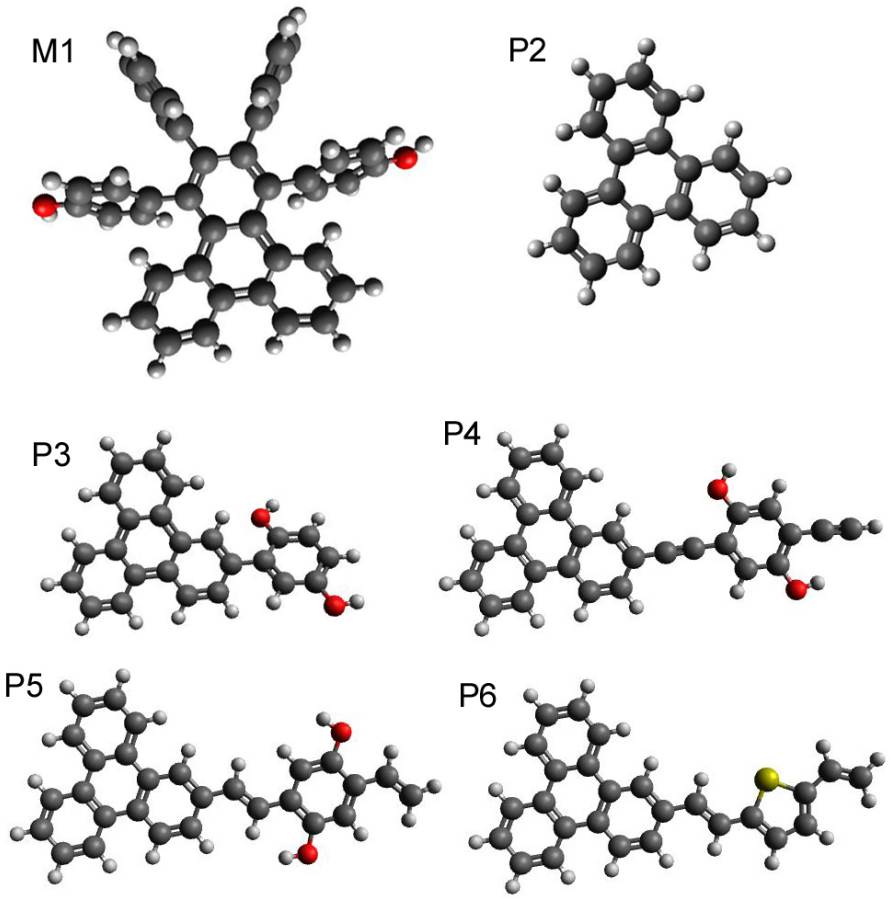

Figure 7: The geometry optimized structures for the basic units: the triphenylene based monomer M1, and polymers P2-P6 (numbering according to corresponding experiment[9])

We suggested that the functional groups that are attached around the triphenylene units in the experiment can be neglected with respect to our purpose of determining the excited states for polymers. This is supported by the electron densities for the HOMO/LUMO and HOMO-1/LUMO+1 which mainly contribute to the lowest excitations. This holds for chains longer than $n = 3$ as exemplified in Fig. 8 with $P2_5$ where the orbitals are delocalized along the chain direction as a consequence of the π-conjugation.

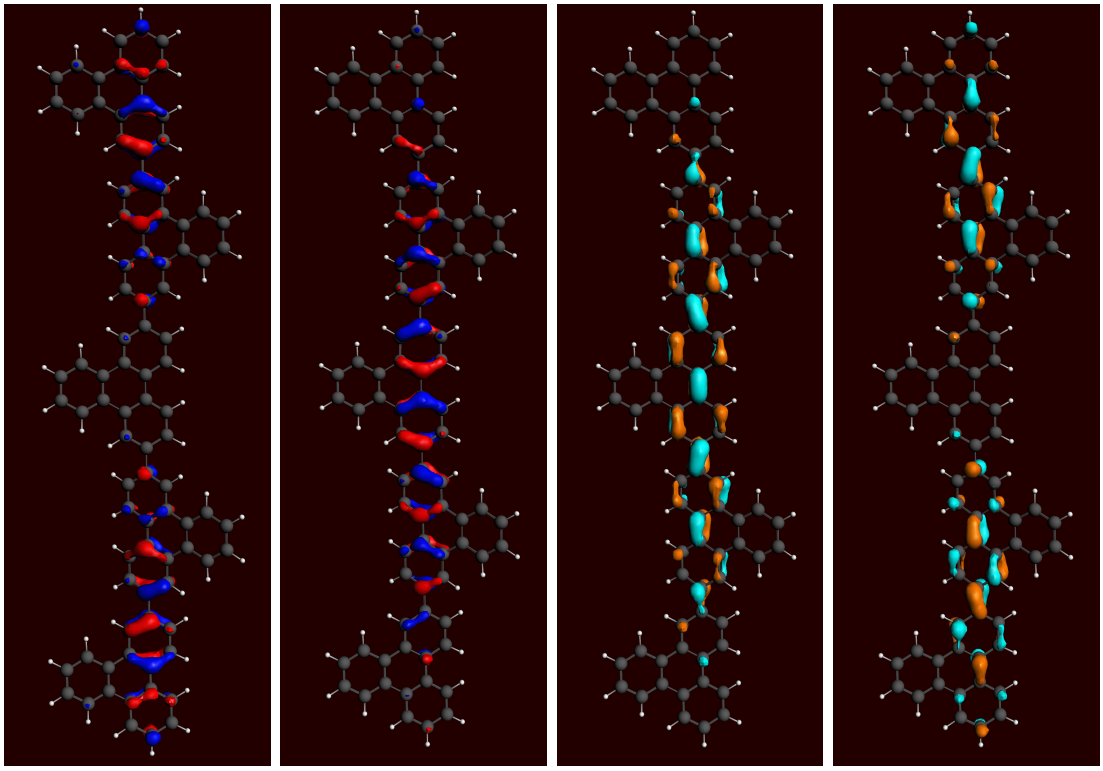

Figure 8: The electron density (generated with ADF) in $P2_5$ for the HOMO-1, HOMO, LUMO and LUMO+1 is located mainly on the inner triphenylene rings along the chain direction. This indicates that additionally attached benzene units to the triphenylene units may play an inferior role.

One may guess that even the outer benzene ring of the triphenylene unit could be neglected regarding electron density and transitions. The simulations on polymer **2** could therefore also be done with pure poly(para-phenylenes)s (PPPs) because the chain geometry is also similar as both types of units are twisted alternately. The dihedral twist angle between triphenylene units (31°) is comparable to that of PPPs (33°). A cross-check calculation for $P2_6$ with a 6-unit PPP polymer showed, that even the relaxed triplet state phosphorescence and the localization behavior is almost the same (see Sec. 3.11). However, as the computational effort for the inclusion of the whole triphenylene unit was possible, we chose to stay with the triphenylene backbone as this was also one of the the key factors in the corresponding experiment.

3.3 Planar vs. Twisted Structures

A previous work of Pogantsch et. al.[78] on the prediction of optical excitations in conducting oligomers indicates, that the twist angle does not change excitation energies significantly. They chose to prefer forced planar geometries as these are also closer to experimental observed packing effects ins solid state geometries, which tend to reduce inter-ring twist.[79]

The polystyrene matrix where the polymers in experiment were dispersed and cooled down to 25 K could impose similar geometric boundary conditions to the examined monomer and polymers. Consequently we suggest that the degrees of freedom for the outer rings of $M1$ in the excited states are defined roughly by the alignment of the ground state geometry - the outer rings may not be allowed to bend out of the plane of the triphenylene unit due to the surrounding matrix.

For $P2$ we tested the effect of forced planar structures (usually the dihedral angle between the triphenylene units is about 33°). The absorption/emission energies for the first excited triplet of planar structures $P2$ lie in average around 0.23 eV/0.13 eV lower than for twisted geometries ($P2_2$ - $P2_6$; see appendix 5.6). These differences in the excitation energies are visualized in the following plots for the B3LYP and LRC-PBE XC functional.

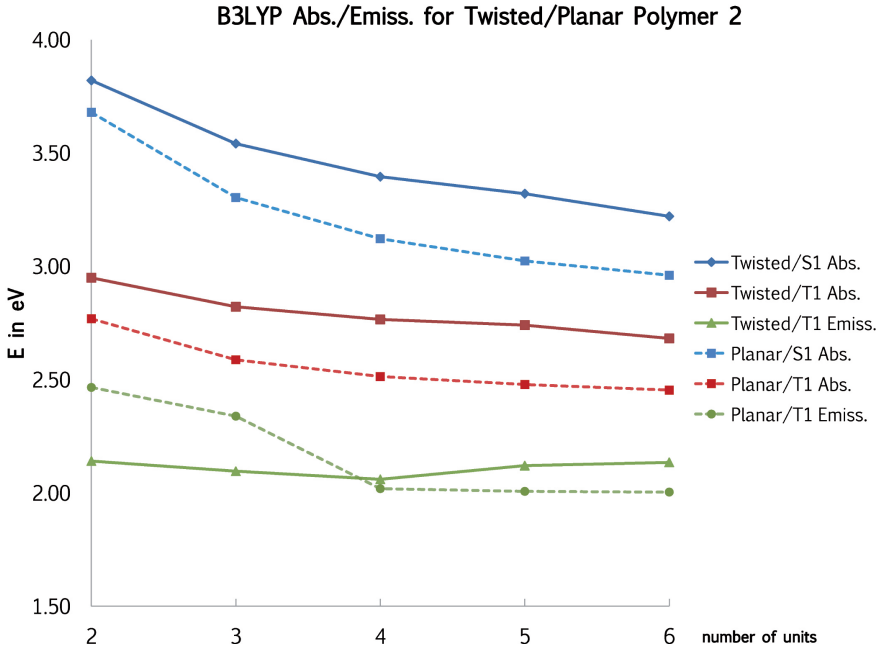

Figure 9: Comparison of absorption and emission energies for twisted and planar triphenylene chains (polymer **2**) using B3LYP. Energies form planar structures are marked with a dotted line and lie in most cases lower.

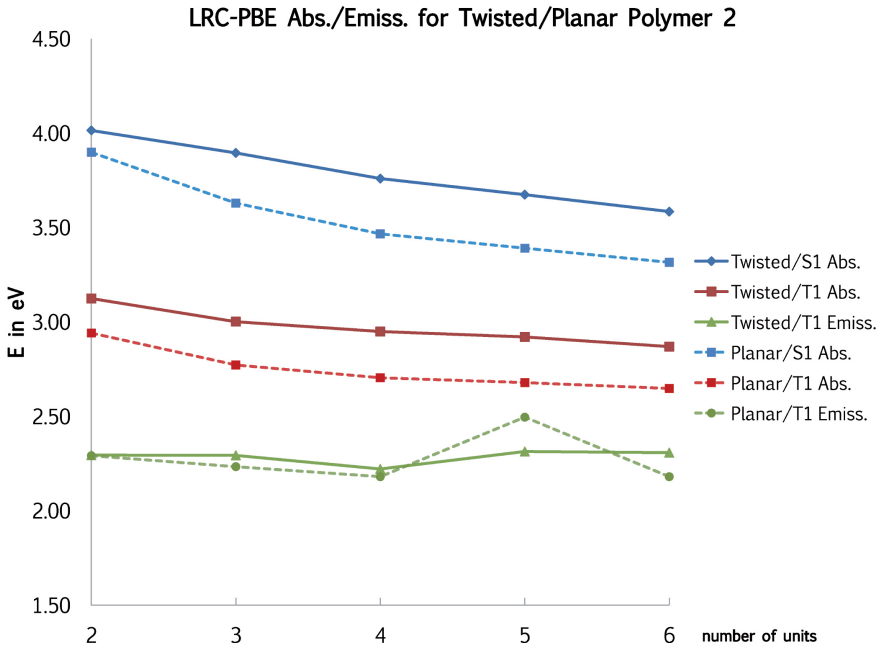

Figure 10: Comparison of absorption and emission energies for twisted and planar triphenylene chains (polymer **2**) using LRC-PBE. Only the T1 emission energies (green) are almost identical for both geometric types; for the S1/T1 absorption (blue/red), the planar structures yield lower energies.

Triplet state localization effects could be observed on both types (twisted and planar) with some differences in the width and exact unit of the localization on the chain (see Sec. 3.11). However we chose not to calculate all polymers twice based on a planar and twisted geometry because the forced planar calculations showed to be sometimes computationally much more expensive than the twisted structures while the general trends could be reproduced with both types. Therefore the 'natural' energetically favored geometry yielding the lowest total energy was used for each type of polymer. This led to twisted geometries for polymer **2** and **3** whereas for polymer **5** and **6** planar geometries showed to be energetically favored. Polymer **4** was problematic in reaching converged geometries for both planar and twisted structures. Energetically the planar structure was favored, but the triplet excited state optimizations often failed to converge or yielded negative excitation energies. By varying the molecular geometry and tracking the potential energy surface (PES) this negative triplet emission energy often indicates that the PES has only a local minimum but not a global. However, this kind of 'error tracking' would have been too time consuming - therefore the geometric excited state optimizations were restarted and the resulting triplet energies were calculated again (if this did't cure the problem, the convergence criteria were set stricter).

Sometimes also the forced planar structure was allowed to bend marginally out of the plane what yielded sometimes reasonable results. The resulting energies are therefore incomplete and useless to compare with the other polymers. Therefore the values for $P4$ are missing in the following graphs. All reasonable results for this polymer are listed only in the tables in appendix 5.
The calculation of the fluorescence energies from the S1, was computationally only possible with the *ADF 2010.02*[68],[69] code if forced planar structures were used. The calculations could due to computationally effort only be finished for $P2$ and partly for $P6$ (up to $n = 4$) which favours energetically the planar structure.

3.4 Computational Details

The basic unit triphenylene was geometry optimized with the exchange-correlation (XC) functional B3LYP[28],[29] using a triple zeta polarized (TZP) basis set with the software *ADF 2010.02* implemented on single workstations. All other ground state geometries were optimized with *NWChem 6.0*.[72] Generally all DFT optimizations used the B3LYP XC functional and a 6-31G* basis set which has an acceptable ratio of accuracy versus computational cost. As any kind of TDDFT excited state geometry optimization was computationally too expensive in *NWChem*, the common method to calculate the triplet geometry by means of ground state DFT was employed.[78] DFT works for excited state states only if the symmetry and spin multiplicity of the excited state is different to the ground state - therefore only the excited triplet geometries are accessible with this method. For the first excited triplet state, a DFT geometry optimization was performed with a spin multiplicity of three leading to an open shell system.[73]
In order to gain the fluorescence energies, a singlet excited state geometry optimization had to be performed in *ADF* as the computational effort in *NWChem 6.0* was too high. This was only possible for the planar $P2$ and $P6$, as the capacities of parallel calculations were limited because the *ADF* code used runs only on single workstations.
Excitation energies accounting for vertical absorption were calculated based on the optimized ground state geometries (S_0). The phosphorescence energies were gained using the first excited state triplet geometry (T_1) - both in *NWChem*. We used one hybrid XC functional B3LYP, the IP-tuned long-range-corrected LC-ωPBE (ω is equal to the tuning parameter γ in the theory part 2.12; the functional is in the following denoted with LRC-PBE), and the semilocal PBE XC functional.[31],[32] For all excited state energy calculations, the Tamm Dancoff Approximation (TDA,[82] in *NWChem* this is called CIS) was

used because there is evidence that this improves the lowest lying singlet and triplet state as explained in Sec. 3.6. Additionally the use of TDA enabled the calculation of longer polymer chains because the memory use in the calculations is significantly reduced because the **B** matrix in Eq. 62 is set to zero.

3.5 Performance Prognosis of the used Functionals

The performance of the standard semilocal functional PBE as well as the common hybrid functional B3LYP was assessed by comprehensive singlet and triplet excited state benchmarks (for the vertical absorption energies based on the ground state geometries) carried out by the group of Jacquemin.[74],[75] PBE is generally not performing very accurate because it consequently underestimates transition energies (about 0.39 eV for singlet, 0.50 eV for triplet) which is partly caused by the too rapid decay of the approximate exchange potentials (see Sec. 2.10). Moreover this leads to a S-T gap that converges zero for long chains which is due to the incomplete cancelation of self-interaction energies[76] and it is also obvious from the long-range behavior of semilocal XC functionals (see Sec. 2.14). This trend is shown in the results for the S-T gaps in Sec. 3.9.
According to Jaquemin et. al., the singlet excited states are best described by hybrids with an HF fraction between 22% and 25%. More or less HF exchange in those functionals lead to an over- or underestimation of transition energies respectively. That is why B3LYP with only 20% of HF underestimates the lowest lying singlet transition energies generally (by more than 0.2 eV). Additionally, in our case the ordering of the two lowest singlet excited states has to be questioned due to some indications shown in the next section.
Another conclusion of Jaquemin, that we could also observe on tests of triphenylene, is that "the statistical impact of using larger basis sets [than TZVP] remains limited".[75] We used different basis sets for the geometry optimization in *ADF* which yielded almost identical results with respect to the bonding lengths. In order to test the basis set dependence for vertical absorption energies, in the following table the differences for DZP, ADZP, TZP and TZ2P are listed.

Triphenylene Basis Set Comparision				
	DZP	ADZP	TZP	TZ2P
			S_1	
PBE	3.65	3.63	3.62	3.62
B3LYP	3.99	3.95	3.94	3.95
			T_1	
PBE	3.25	3.23	3.23	3.23
B3LYP	3.02	3.01	2.99	3.00

Table 1: Vertical absorption energies (in eV) for the first excited singlet (S1) and triplet (T1) states of triphenylene calculated with TDDFT by use of different basis set sizes. The resulting energies do not differ much indicating that the computational fast DZP basis set yields converged results within an acceptable accuracy.

Whereas for singlet excited states, the fraction of HF mixing is directly linked to the quality of the results, triplet excited states are not governed mainly by this parameter.[75] Furthermore the general trend is that most functionals have larger deviations for triplet than for singlet excited states. The hybrid B3LYP is listed to underestimate the values by more than 0.4 eV.

As the S-T gaps for the vertical absorption couldn't be compared with an experiment that measures the emissions, the cited performance analysis gives just a rough idea about accuracy. The results for the S-T gaps in absorption are shown in Sec. 3.9 and confirm the range of underestimation.

3.6 Ordering of the two lowest Singlet States

Special attention was paid to the two lowest singlet excited states. One of these, which is commonly denoted with L_a is contributed mainly by the HOMO->LUMO excitation. The other one, L_b consists by more or less equal parts of the HOMO-1-> LUMO and HOMO->LUMO+1 transition.[77]

For linear acenes as well as triphenylene and also some nonlinear PAHs (Poly Aromatic Hydrocarbons), the L_a is stated to have a charge-transfer (CT) character, whereas the L_b is covalent like the ground state.[77]

To find out whether one of the first excited states is charge-transfer like is important because it has long been known,[16] that TDDFT predicts those energies with large errors increasing with the system size.[78] Even for linear acenes, which have no real long range CT states (no CT actually happens),[80] the L_a is wrongly predicted by TDDFT on the

B3LYP level leading to a wrong ordering of L_a/L_b.[81] In these linear acenes the L_a state is described to have an 'ionic character' as a special case of CT for which the wrong long-range behavior of standard semilocal functionals cannot account for. One suggestion to treat such weak' CT cases is to use the Tamm Dancoff Approximation (TDA)[77] which is also favorable because it reduces computational efforts.

In order to determine whether a transition is charge-transfer like or not, there have been made several approaches.[84] The logical relation between the spatial overlap of the contributing orbitals and a CT state was described by a specific formula (first introduced by Peach et. al.[85]). But this popular 'CT-Metric' was found to be not well-defined as one has to find the unitary transformation to minimize the spatial overlap.[86] Without this transformation applied, the formula cannot be used universally as it led to wrong predictions in some cases (Acenes: CT-Metric for L_a even better' than for L_b[80],[86]).

Otherwise, several calculations showed,[80],[84],[85] that some sophisticated long-range corrected (LRC) hybrid functionals decrease the well known error for CT states; in some cases even it's system size dependence.[84] Therefore the best method to determine whether the results of a TDDFT excited states calculation can be trusted is to do some diagnostic calculations for the L_a with sensible LRC functionals. If the L_a states show a deviation, it should be considered that the L_b state is the real lowest singlet state. Yet, if this is true, the value of the L_b should not be taken from the LRC calculation as it is predicted less accurately by LRC functionals with respect to non-LRC functionals.[75],[77],[84] Additionally one needs to be careful with triplet states from LRC functionals as they can be sensitive to instabilities in the ground state[75] - but this may be cured by using the LRC tuning parameter ω plus the TDA.[87] Therefore this was another reason for the usage of TDA in our calculations.

For the $P2_4$ and $P2_5$ triphenylene chain we performed test calculations of the vertical excitation energies to find the ordering of the lowest excited states with different LRC functionals: LRC-μBLYP and LRC-ωPBE with IP-tuned range-separation parameters ω and μ (parameter notation as implemented in *NWChem 6.0*, see also Ref.[87]) which are basically the same as the parameter γ in Sec. 2.12. For all other polymers we used only the LRC-ωPBE functional. Comparing the transition energy values to LRC-μBLYP shows that both functionals yield similar results.

	$P2_4$		$P2_5$	
	LRC-BLYP	LRC-PBE	LRC-BLYP	LRC-PBE
S1 (abs.)	3.74	3.76	3.68	3.68
T1 (abs.)	2.96	2.95	2.94	2.92
T1 (emiss.)	2.19	2.22	2.73	2.31

Table 2: The absorption (abs.) energies (in eV) of the excited S1 and T1 state for polymer $P2_4$ and $P2_5$ are very similar for the two semilocal long-range-corrected XC functionals LRC-BLYP and LRC-PBE. Only for the T1 emission differences occur ($P2_5$).

The calculations of all polymers show that the investigated polymer chains generally don't show a wrong ordering of the two lowest excited singlet states. This is also underlined by the strong oscillator strengths for the S1 states whereas the S2 states are mostly weak. Only one molecule, $P2_3$, switches its lowest lying singlet states when using the LRC-PBE functional instead of B3LYP and PBE. This can be identified by the orbitals which contribute for the transition, whether they have an L_a or L_b character as described above. The molecules that showed always this switched L_a/L_b ordering for each XC functional are the monomer M1 and the 2-unit triphenylene $P2_2$ as well as the basic unit $P3_1$ (see appendix 5.7). However, our choice of 'lowest' singlet excited state was ruled by the strongest oscillator strength (corresponding mostly to the L_a), because the emissions in the experiment are also strong.

3.7 Excitation Energies and the Spectra

In TDDFT there are different energies accessible that can be compared to experiment. The Franck-Condon principle accounts for the transition behavior in detail as electronic transitions are very fast compared with the time scale of nuclear motions. Therefore the vibrational levels of the excited state must be instantaneously compatible. The so-called Franck-Condon factor contributes to the transition probability: the vibrational overlap integral of the initial and final state. It is an approximation as it incorporates the Born-Oppenheimer approximation and uses the electrical dipole transition assumption, but it accounts very well for the general spectroscopic behavior. In this work there were no vibrational levels included and the nuclei are treated classically as 'fixed'. The inclusion of vibrational levels would have led only to minor corrections within the usual accepted error range of TDDFT (0.1-0.2 eV)[74],[75] while it would have demanded much more computational effort. However the basic principle of the difference of vertical absorptions and

vertical emissions in the relaxed geometry (fluorescence and phosphorescence as schematically depicted in Fig. 11) can be reproduced also without the inclusion of vibrational excitations.

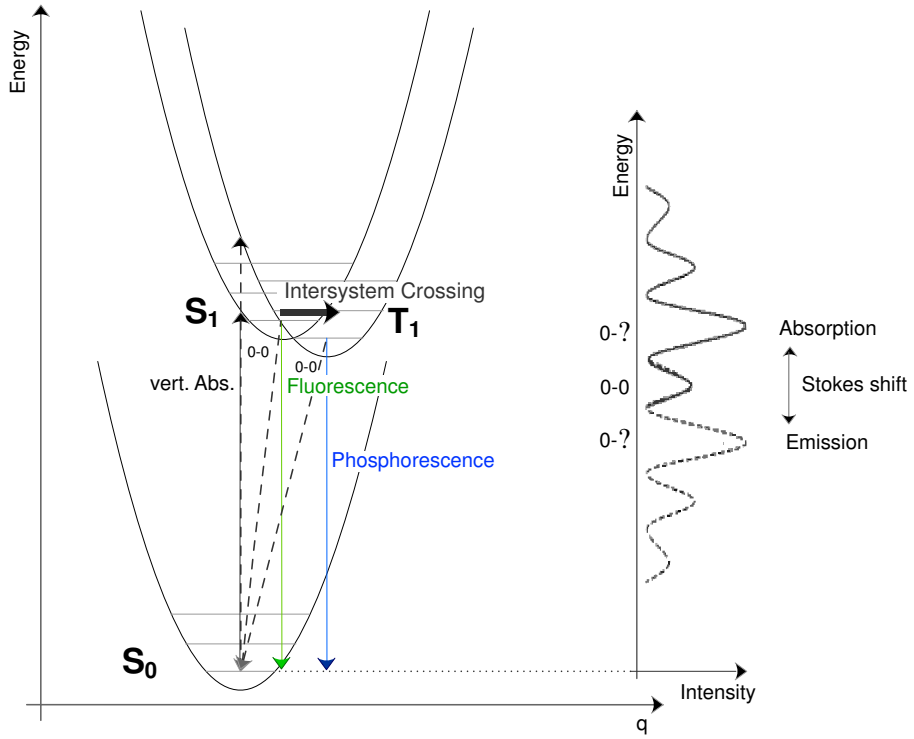

Figure 11: The sketch shows adiabatic energy curves for the initial ground state S_0 and final states S_1 and T_1 with an energy minima related to the reaction coordinate q - for different excited states the molecule relaxes into different geometries. The schematic spectra shows the relation to the absorption, 0-0 energy and emission like fluorescence, phosphorescence and the Stokes shift.

The maximum of absorption is approximated by the vertical transition energy, which can be expressed by the difference of the total energy between initial (S_0) and final (S_n) states while the molecular geometry stays the same. For the vertical absorption into the S1 or spin forbidden T1 this would be

$$\nu_{vert}^{abs}(S_1) = S_{1(S_0)} - S_{0(S_0)} \tag{81}$$

$$\nu_{vert}^{abs}(T_1) = T_{1(S_0)} - S_{0(S_0)} \tag{82}$$

where the subscript denotes the geometric state of the molecule (the molecular geometry can be relaxed into the ground state S_0 or an excited state S_n / T_n).
Practically the vertical absorption energies in each geometric state are calculated by means

of an TDDFT excited state calculation. TDDFT basically only accounts for vertical absorptions but not for emission energies. However, emission energies can be accessed indirectly by performing TDDFT calculations based on the different molecular geometry of the excited state. The phosphorescence (vertical emission) can therefore be expressed as

$$\nu_{vert}^{emiss}(T_1) = T_{1(T_1)} - S_{0(T_1)}. \tag{83}$$

Similar, the fluorescence energy based on the related S1 geometry is: $\nu_{vert}^{emiss}(S_1) = S_{1(S_1)} - S_{0(S_1)}$. These values can then be compared to the maxima in the emission originating from the experiment (see Fig. 5).

As already explained in Sec. 3.4 the relaxed S_1 geometry calculations could only be performed for polymer **2** and **6**. One result is that the Stokes shift of planar structures is in average 0.29 eV for $P2$ and 0.55 eV for $P6$. However this can't be compared to experiment because only emissions were measured.

The experimental fluorescence energy is 3.02 eV for $P2$ whereas the comparable $P2_6$ planar structure only reaches 2.68 eV (with B3LYP). The best calculated value for the experimental phosphorescence of $P2$ with 2.39 eV is reached with the twisted $P2_6$ geometry and LRC-PBE functional yielding 2.31 eV. In consistence with the experimental finding, only the T_1 geometries showed a clear localization behavior compared to only slightly changed S_1 geometries (see Sec. 3.11).

Another value that can be compared to the experiment is the 0-0 onset energy lying energetically between emission and absorption as sketched in Fig. 11. The 0 denotes the lowest vibrational level. This 0-0 energy is defined to be

$$\nu_{0-0}^{emiss}(T_1) = T_{1(T_1)} - S_{0(S_0)} = S_{0(T_1)} - S_{0(S_0)} + \nu_{vert}^{emiss}(T_1) \tag{84}$$

and $T_{1(T_1)}$ is only accessible indirectly via Eq. (83) demanding a TDDFT calculation based on the T1 molecular geometry (a TDDFT calculation yields only vertical absorption energies). So practically the last term is taken from the TDDFT T_1 energy at the relaxed T_1 geometry and the total ground state energies of the relaxed geometries can be accessed in the output files. The 0-0 energy is not visualized in the following in order to keep the plots clear, but they are listed in the appendix. As not all calculations for the 0-0 energy did finish or converge, the tables in appendix 5 are incomplete.

Characteristically the 0-0 energy calculated with PBE is often wrongly too low indicating that the optimized triplet state geometry has not reached a global energetic minima. The

other results from LRC-PBE and B3LYP don't show this behavior and the 0-0 energy lies correctly in between the absorption and emission energy. Therefore the usage of the PBE XC functional for triplet geometry optimizations is not advisable. Values for all kind of resulting excitation energies are listed in appendix 5.

3.8 LRC Parameter Scaling

In literature, the scaling of the characteristic range-separation parameter γ with the length is for highly conjugated chains found to scale linearly with the inverse chain length.[62] For sufficient long chains this would lead to a vanishing small LRC parameter leading to the pure semilocal GGA. However due to experimental observed localization effects, we expected the LRC parameter to saturate with an increasing chain length. This is confirmed for the polymer types we calculated.

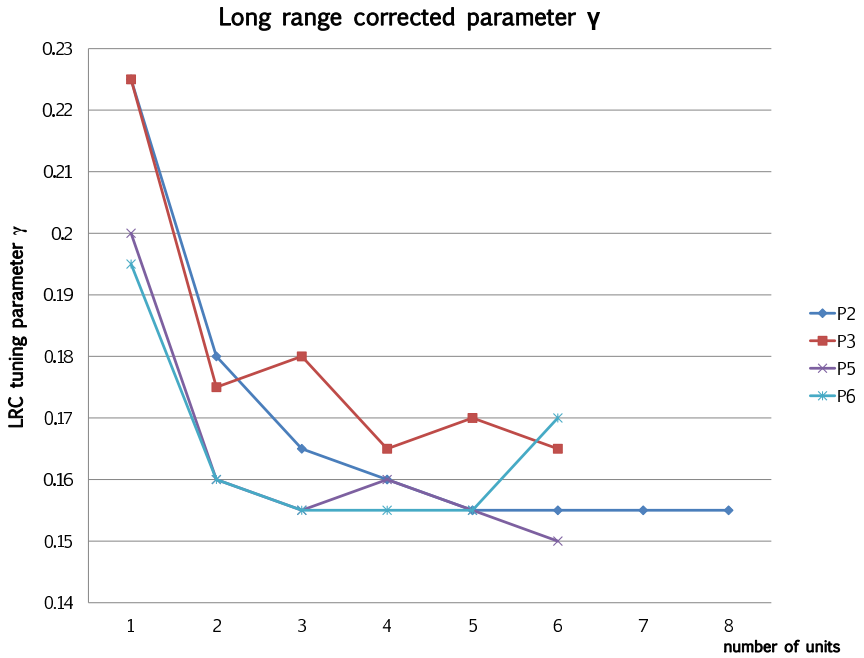

Figure 12: The LRC parameter γ seems to saturate' with increasing polymer length within the range of 0.15 and 0.17

The LRC parameter for the polymer types varies for chains longer than n=4 between 0.15 and 0.17, instead of converging to zero. Due to the connection of the LRC parameter with the ionization potentials (see Sec. 2.12) which in turn leads to an improved consistency of HOMO energies with the IP theorem, the saturating tuning parameter reveals the similar

range of the ionization potential and the HOMOs.

3.9 Results from Absorption Energies

In this section the schematic trends for the S-T absorption gap, the S_1 absorption energy and oscillator strength are shown. The S-T emission gap (which was measured in the experiment[9]) couldn't be gained for all polymers, because the S1 emission energies were computationally only accessible for the planar triphenylene chain (P_2) and partly P_6 (see Sec. 2.15). Only the *ADF* code could be utilized to calculate the singlet excited state geometries, what restricted the XC functional to B3LYP because LRC functionals are not included in the code. In this section, only the results from absorption energies are shown.

Using the PBE XC functional leads to a S-T absorption gap converging to zero as expected (see Sec. 3.5). In contrast, the S-T gap 'saturates' for functionals with a fraction of HF exchange (LRC-PBE and B3LYP) shown in the following figures.

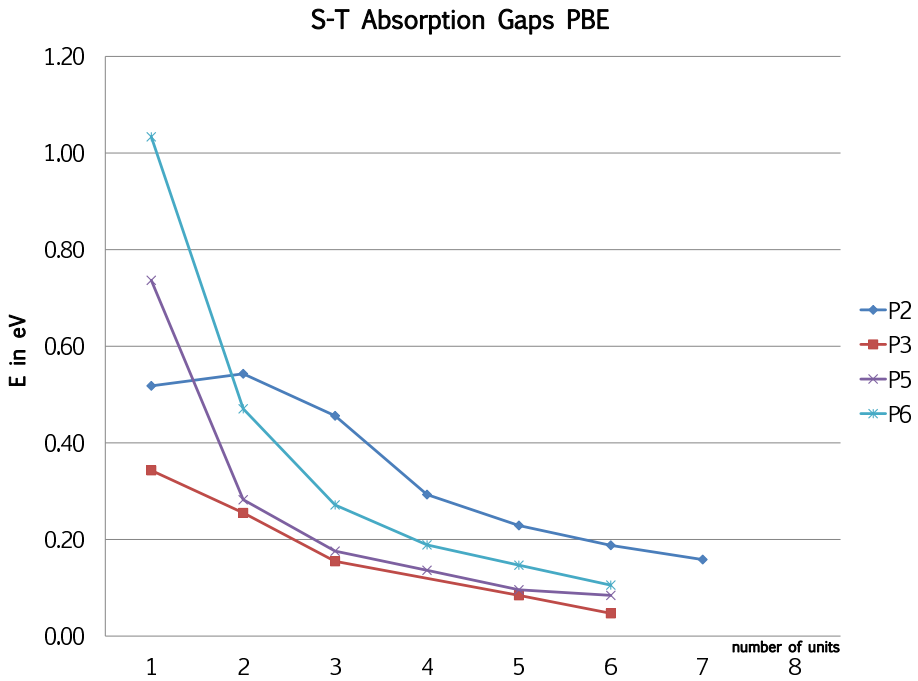

Figure 13: The S1-T1 absorption energy differences (S-T gap) converge to zero for the PBE XC functional for all types of polymers

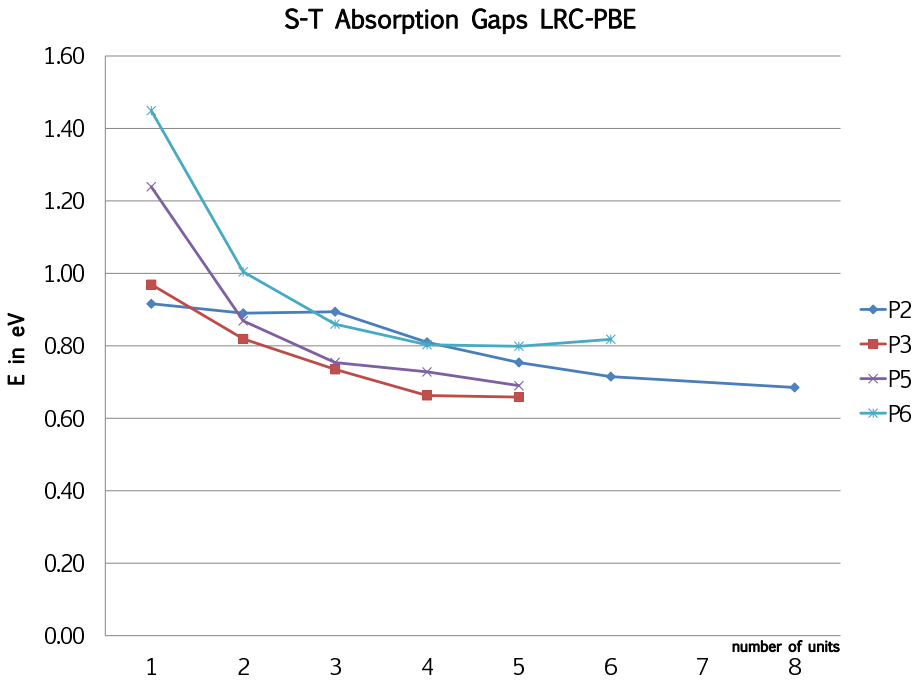

Figure 14: Using the LRC-PBE XC functional leads to a S-T absorption gap that converges to a finite value between 0.62 and 0.82 eV

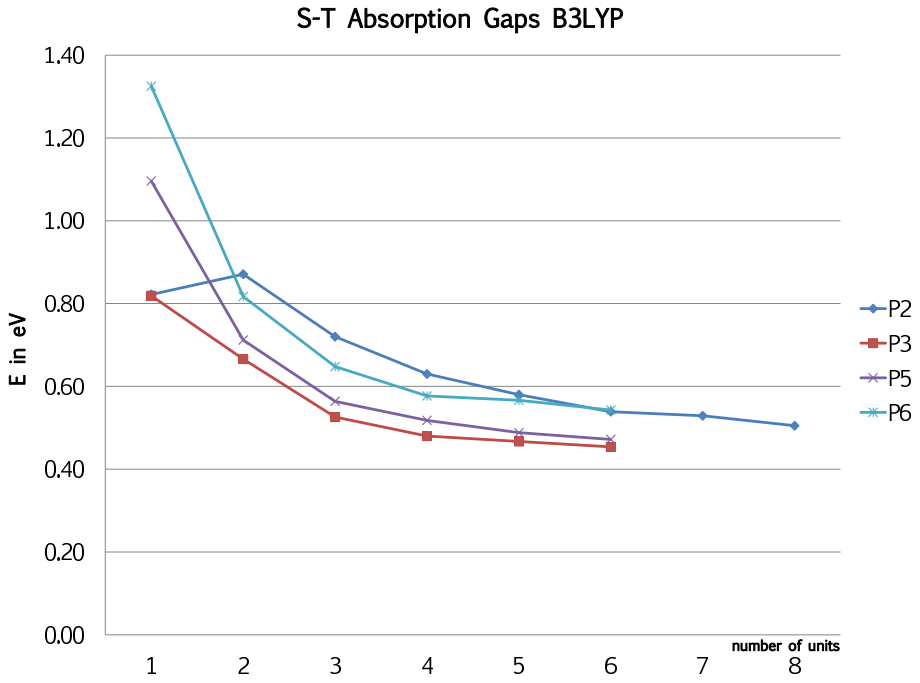

Figure 15: With B3LYP the S-T absorption gap is always lower than with LRC-PBE but it also saturates at a finite value between 0.4 and 0.6 eV

In the experiment[9] there is found a relative ordering of the polymers with respect to the S-T gaps. From monomer **1** to polymer **6** the S-T gap is decreasing: 0.76 eV for the monomer shrinking to almost zero for polymer **6** (see also Fig. 5). This behavior is not reproduced in the calculated S-T absorption gaps as plotted in the figures above. Absorption and emission excited state energies differ significantly (Stokes Shift) as shown in Sec. 3.7 what is one reason why this relative ordering is different. Another reason is, that the triplet localization in the calculations is still different to the observations in experiment as explained later (see Sec. 3.11).
In order to compare trends of the S_1 absorption energies with respect to S_1 emission energies in experiment, the next table lists these S_1 absorption values for the longest calculated polymer for each type along with the experimental values in emission. For $P2$ and $P6$ also the resulting S_1 emission energy from the *ADF* singlet excited state calculation is listed. These energies underestimate the experimentally observed values by more than 0.4 eV.

Polymer	B3LYP (abs.)	B3LYP(emiss.)	LRC-PBE (abs.)	exp. (emiss.)
M1	3.8	2.67	3.9	3.1
P2	3.2	-	3.5	3.0
P3	3.1	-	3.5	2.9
P4	2.5	-	2.9	2.8
P5	2.2	-	2.6	2.6
P6	2.2	1.95	2.6	2.4

Table 3: Vertical absorption energies (in eV) for the first excited singlet (S1) states of all polymers - each using the longest calculated chain size ($n = 6$ for $P2$ both abs./emiss., $n = 5$ for $P3$ and $P5$, $n = 6$ for $P6$ (S_1 abs.), $n = 4$ for $P6$ (S_1 emiss.)). The S_1 absorption energy is decreasing systematically from M1 to P6 what matches the relative trend from experiment despite the difference that emissions were measured.

The relative ordering of the absorption energies is the comparable to the experiment: the monomer has the highest S_1 energy and polymer 6 the lowest. The values of the S_1 energies can't be compared, as absorption energies lie always higher than emission energies.
As already explained in the theory part (see Sec. 2.15), the oscillator strengths are expected to scale linearly with the chain length for XC functionals that include HF exchange (B3LYP and LRC-PBE). The results from TDDFT absorption calculations confirm this for all polymers. The following figure plots this scaling behavior of the oscillator strength for

polymer **2** using different XC functionals.

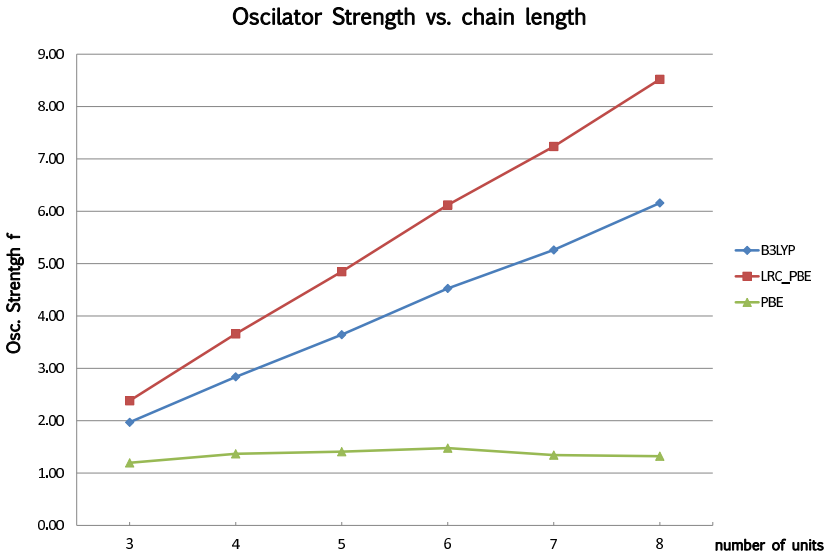

Figure 16: Oscillator strength of the first excited singlet state versus the chain length of the triphenylene polymer **2**. Only XC functionals with a fraction of Hartree-Fock (B3LYP and LRC-PBE) show the correct linear scaling.

3.10 Transition Energies

In this subsection the main results for TDDFT excitation energies for all polymers are shown and compared to experiment.

For the monomer, the TDDFT T1 emission energies (phosphorescence) can be directly compared to the value 2.37 eV gained by the group of Lupton;[9] all energies are listed in the following table.

Monomer 1	**PBE**		**B3LYP**		**LRC-PBE**	
	Abs.	Emiss.	Abs.	Emiss.	Abs.	Emiss.
S1	3.18		3.76		3.88	
T1	2.84	1.95	3.02	2.05	3.14	2.06

Table 4: S1/T1 absorption energies and T1 emission energies (in eV) for the monomer $M1$; the experimental phosphorescence value is 2.37 eV[9]

The triplet geometry optimization favors a structure, where the outer rings are bended out of the plane where the triphenylene is located. As we suggest the polystyrene matrix to prevent those kind of extreme torsions at 25K, we fixed the dihedral angle of the outer rings to the inner triphenylene plane during the optimization (otherwise the phosphorescence energy would be only 0.16 eV for B3LYP which is much too low). The resulting T1 emission energy of 2.06eV for LRC-PBE shows the highest accuracy compared to the experimental value of 2.37 eV.[9]
The vertical absorption and emission energy $\nu_{vert}^{abs}(T_1)$ and $\nu_{vert}^{emiss}(T_1)$ are shown in the following figures for all polymers (only polymer **4** is missing as explained in Sec. 3.3) calculated with different XC functionals.

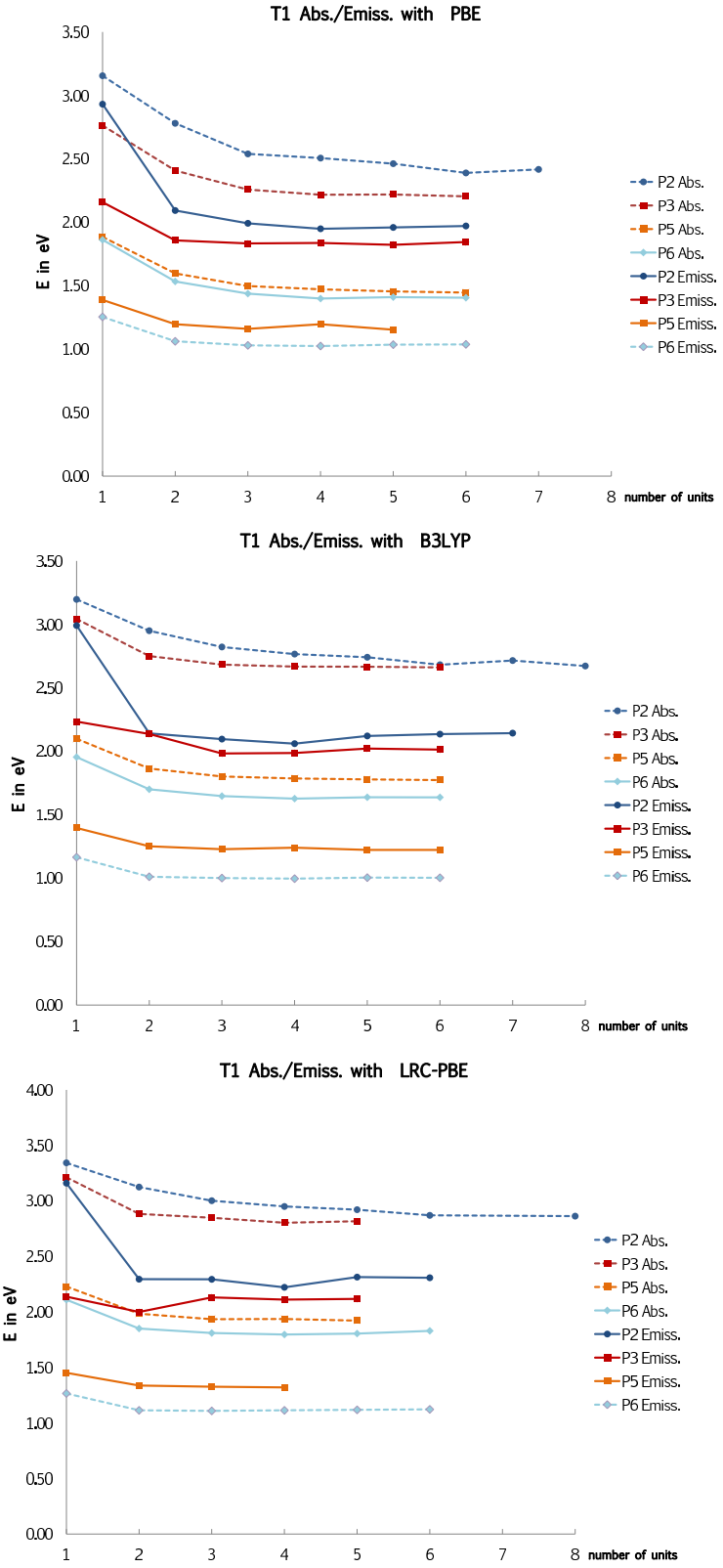

Figure 17: T1 abs./emiss. energies with increasing polymer length using PBE, B3LYP and LRC-PBE. The triplet emission energy depends on the type of polymer.

A saturation of the triplet excitation energies with the chain lengths can be observed for all types of polymers. However the phosphorescence energies of all kind of polymers do not converge to a fixed value - they differ by more than 1 eV for the different polymer types. This is in contradiction to the observations of the group of Lupton[9] (see also spectra in Fig. 5) - their suggestion is that a similar localization behavior on one triphenylene unit for each polymer leads to a fixed phosphorescence energy. Indeed, localization is observed for the triplet excited states in the calculations as well, but it is not localized on the triphenylene units but on the bridging units (see Sec. 3.11 for details).
The next figures show the T1 absorption and emission energies with respect to the different used XC functionals.

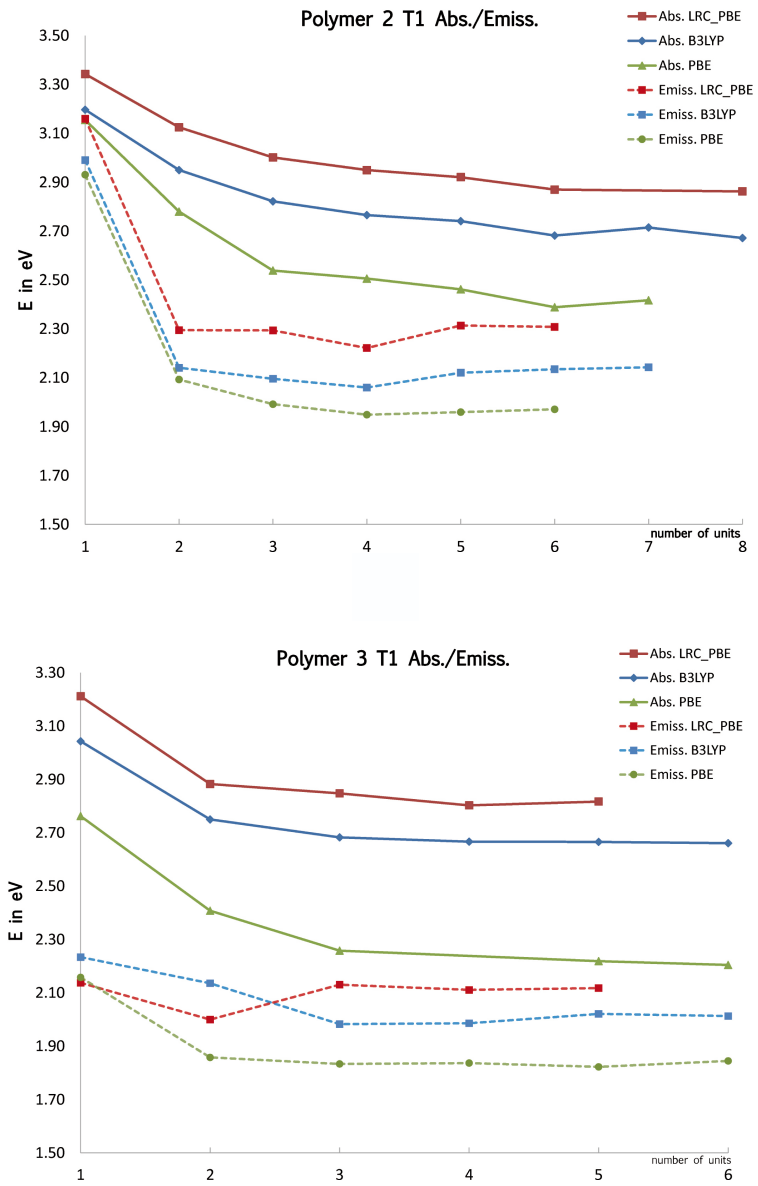

Figure 18: The T1 absorption and emission energies vs. increasing chain lengths for polymer types $P2$ and $P3$ with respect to different types of XC functionals. In the experiment[9] there is only the triplet phosphorescence measured at a almost fixed value of 2.37 eV for *each* polymer type. This behavior is not reproduced, but the highest accuracy to this value is gained by the LRC-PBE XC functional for the pure triphenylene polymer $P2$ reaching 2.31 eV for $n = 6$.

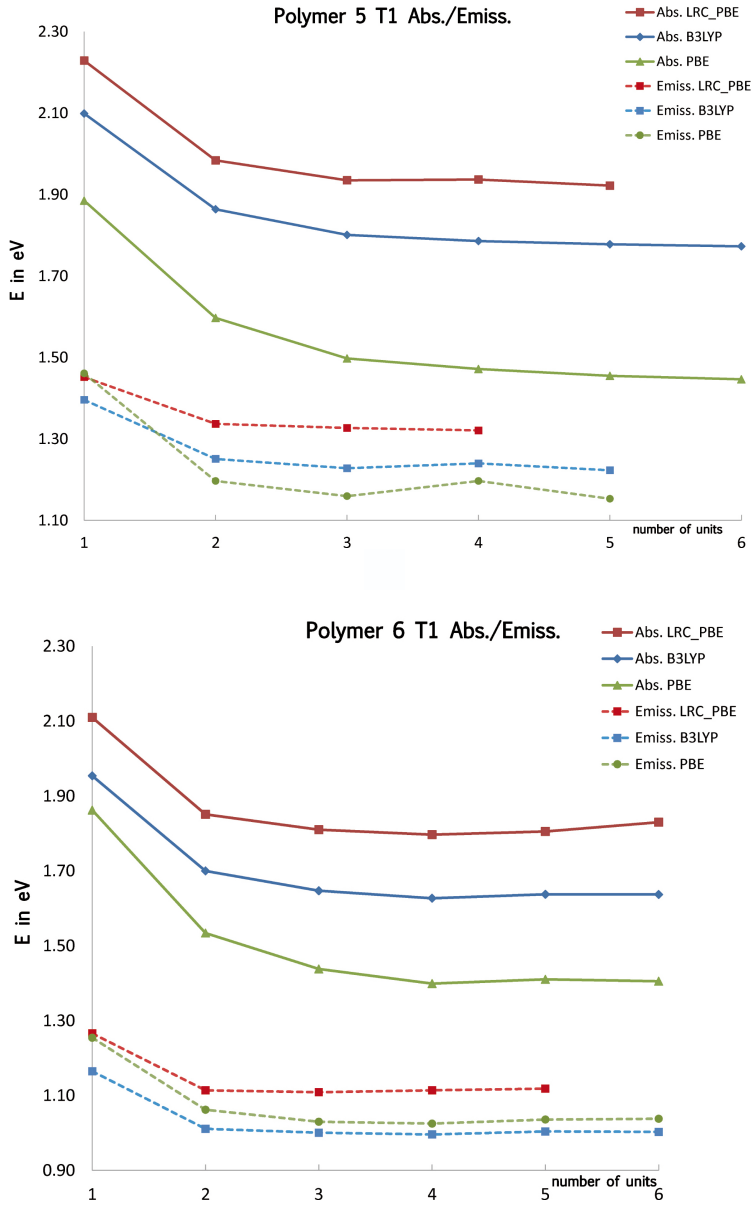

Figure 19: T1 absorption and emission energies for polymer types $P5$ and $P6$ for XC functionals PBE, B3LYP and LRC-PBE.

The tables for all kinds of calculated excitation energies (S1/T1 Abs./0-0/Emiss.) are listed in appendix 5.

Polymer **2** with n=5 showed in the first calculations some unsystematic differences to the above plotted results. The T1 emission energies for all XC functionals were significant higher than for n=4 and n=6. This was because the triplet state geometry optimization found a local minimum for the total energy but not a global. After converging the calcu-

lations for $P2_5$ again, a geometric constellation with an lower total energy was reached, what then reproduced the systematic results shown in Fig. 18 above.

3.11 Localization Behavior

Characteristic for triplet excited states is the switching of some single and double bondings. For the basic unit triphenylene this is shown in Fig. 20.

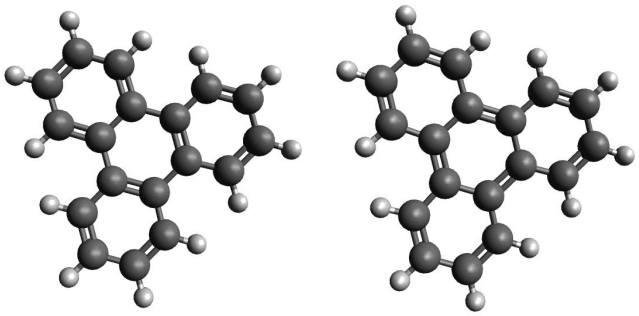

Figure 20: Some single and double bondings switch in the first excited triplet state geometry (right) compared to the ground state (left) for triphenylene, other bonding lengths differ as well but this can only be seen by comparing the numbers directly. Both geometries were optimized with *ADF* using the B3LYP XC functional.

Following the graphical visualization of the changes in carbon-carbon bond lengths in Ref.,[78] the localization manifests itself in systematical deviations of these bond lengths (by comparing the same C-C bondings 'paths' as sketched in the following figures) for the ground state (GS) and the triplet excited state geometries. The absolute differences between the C-C bonding length of the ground state (GS) and the first triplet excited state with respect to the used XC functional is plotted. The localization effects are showing a systematic behavior for polymers with length $n > 3$ what is linked again to the smaller influence of the outer rings in longer chains.

The following graphs visualize triplet localizations for the longest calculated polymers of each type (triplet localization is also observed for shorter chains, but clearer visible in the longer chains which are also better approximations to the experiment). Not each type of the three XC functionals (PBE, B3LYP and PBE-LRC) did finish with respect to calculation time and convergence, but the general behavior of these functionals becomes clear.

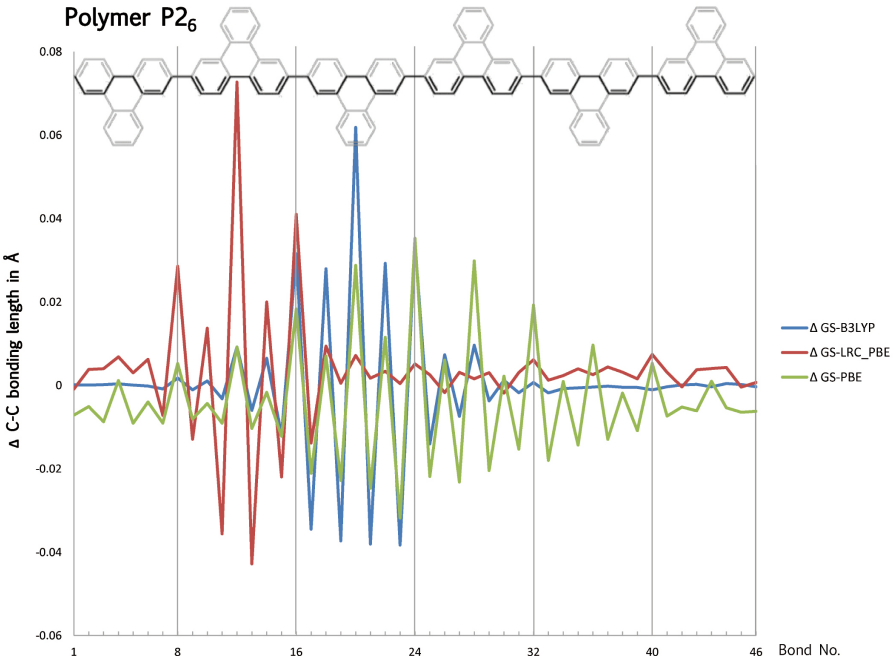

Figure 21: The C-C bonding lengths are measured along the sketched path of the polymer $P2_6$. The absolute difference to the ground state (GS) bonding length shows where bonds get tighter (positive value) or looser (negative value). A clear localization is seen on the 2nd triphenylene unit for LRC-PBE and on the 3rd unit using B3LYP, whereas the PBE XC functional doesn't show a clear localization pattern.

The interesting difference in the localization behavior between triphenylene and the other triphenylene-like polymers is that the latter tend predominantly to localize on the 'bridging' units in between the triphenylene backbone as visualized in the following figures 22 - 24. The triplet geometry using the PBE XC functional did only converge for $P6$.

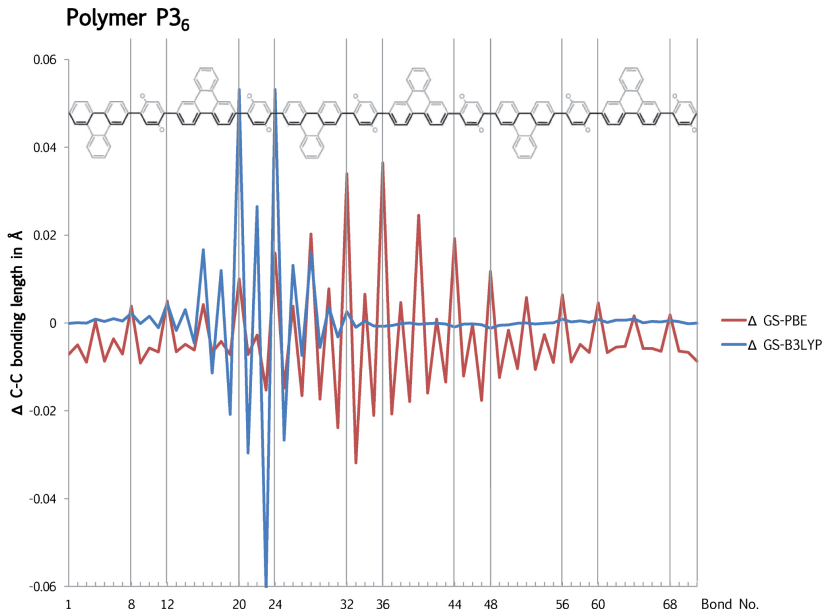

Figure 22: The triplet localization of $P3_6$ occurs mainly on the second bridging unit 1,4-benzoquinone for B3LYP whereas PBE shows a smeared and weak localization in the middle of the chain

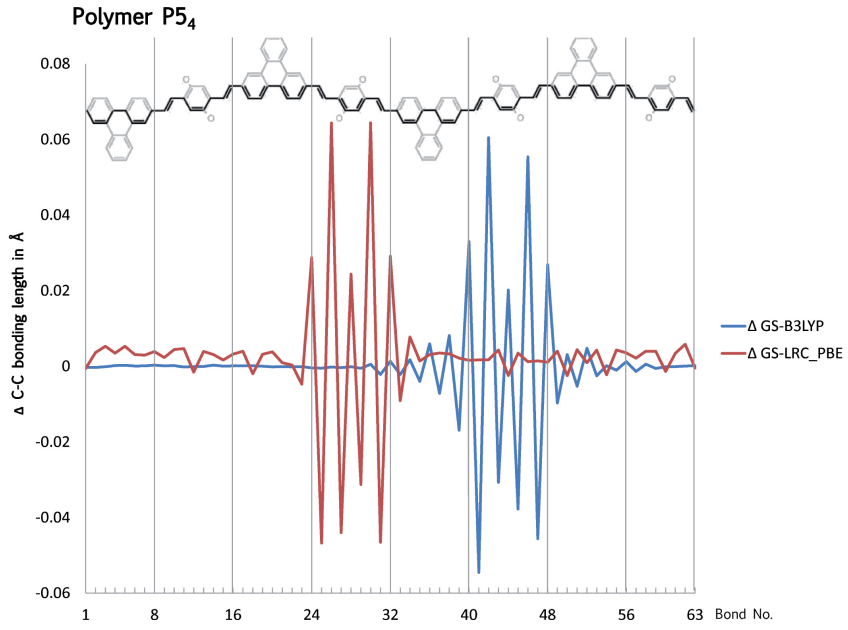

Figure 23: The triplet localization of $P5_4$ concentrates around the bezoquinone units (2nd 'bridge' for B3LYP, 3rd 'bridge' for LRC-PBE).

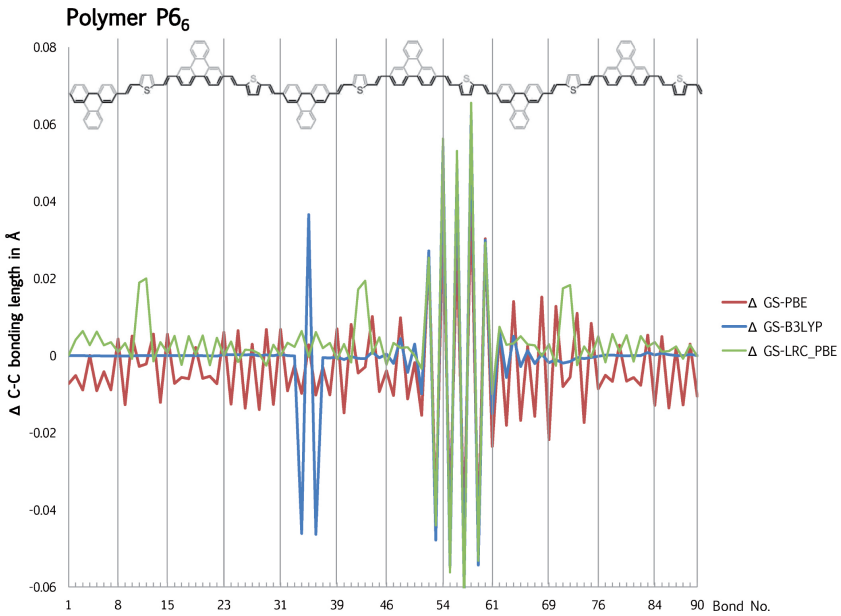

Figure 24: The triplet state of $P6_6$ is located mainly on the fourth thiophene bridging unit by using B3LYP and LRC-PBE whereas the same pattern is much weaker and more smeared with PBE.

This explains, why the phosphorescence energy for the polymers P3 - P6 differs significantly (more the 1 eV, see Fig. 17) from the pure triphenylene chain P2 phosphorescence energy. This is in contradiction to the results from the experiment of the group of Lupton[9] - the experimental observations indicate that the localization on the triphenylene unit is predominant for all kinds of triphenylene based polymers what explains the fixed' phosphorescence energy. Reasons for this discrepancy are discussed in Sec. 3.12.

Concerning the performance of the different used XC functionals, the clearest localization of the first triplet excited state on a certain region of the polymer is reached with the LRC-PBE XC functional. It also yields the T_1 emission values closest to the values from experiment. With respect to accuracy this confirms that a long-range-corrected XC functional is often the best choice.
A clear localization is also found with the hybrid B3LYP, but the phosphorescence values underestimate the experimental results slightly more than with LRC-PBE.
With PBE the localization is not clearly located, smeared over many units and the TDDFT triplet emission energies are much too small. The triplet excited state geometries are often not converged what can be seen from the total energy which has not reached a global minimum. This shows that PBE is not advisable as the inclusion of HF exchange (hybrid)

or better 100% at long ranges (LRC) in the XC functional is essential.

For completeness, the localization behavior of the longest calculated planar $P2$ chain is also visualized, confirming that the choice of using 'naturally' twisted structures may describe the experiment better, because LRC-PBE locates only there correctly on a triphenylene unit instead of in between two units.

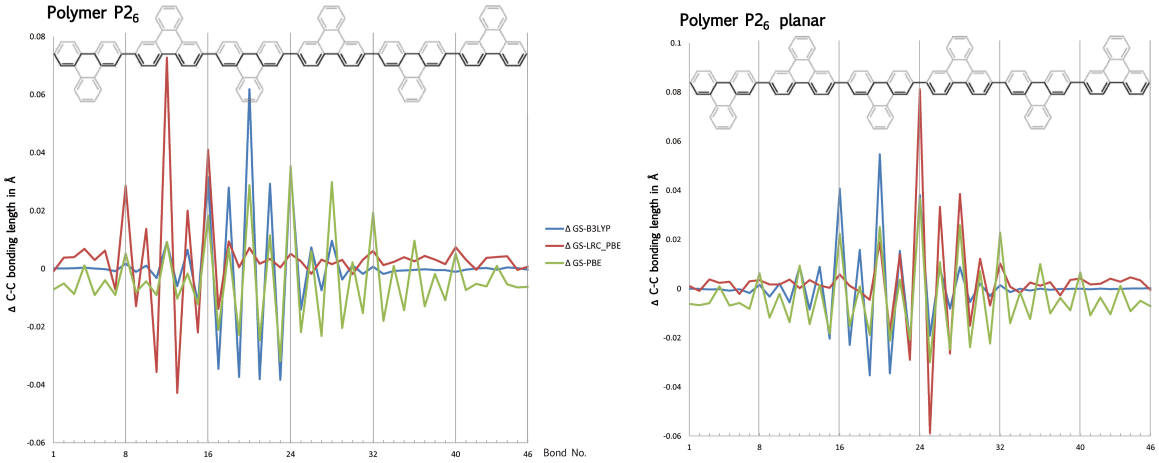

Figure 25: Comparison of the localization patterns of the same polymer $P2_6$ for a twisted structure (left) or planar structure (right). B3LYP and PBE show a similar localization pattern whereas LRC-PBE locates in between two triphenylene units. The energetically preferred twisted structure machetes the observations from experiment better (localization on the units, not in between).

Concerning the localization behavior of the first singlet excited state, the geometric deviances from the ground state for $P2_6$ yields the same result than the experiment as depicted in the following figure. The singlet excited state geometry (S1) is smeared over several triphenylene units whereas the triplet (T1) is more localized.

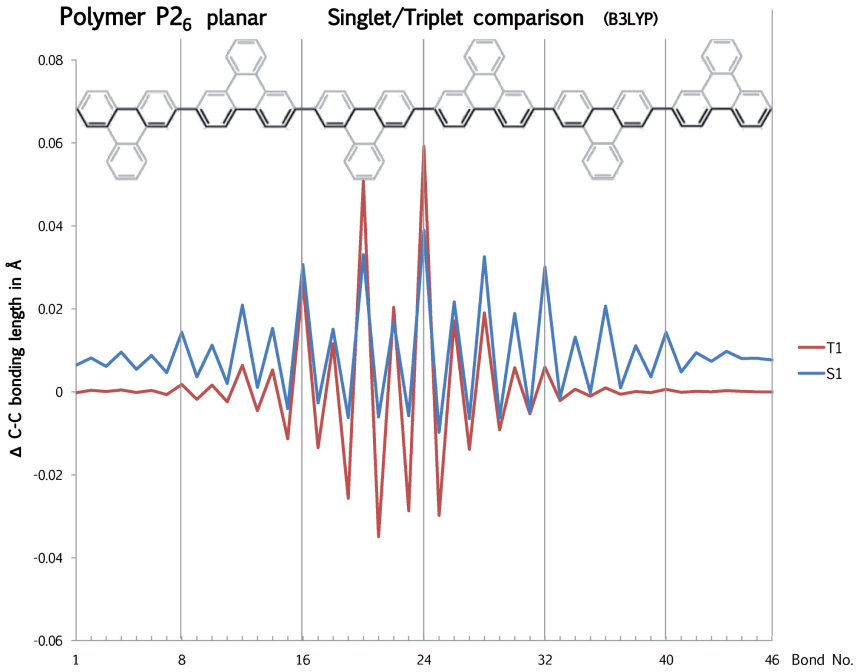

Figure 26: For $P2_6$ S1 and T1 excited state geometries are compared using B3LYP: The triplet state shows a clearer localization behavior whereas the S1 is more delocalized. Overall, in the T1 state the bonding lengths are tighter.

Picking up the idea of a pure poly-para-phenylene (PPP) chain in Sec. 3.2 again, the localization of the triplet excited state of the PPP-chain corresponding to the pure triphenylene chain $P2_6$ is shown next. The similar localization pattern is obvious for B3LYP and LRC-PBE but the existence of the triphenylene structure forces the localization to shrink always the C-C bonding in the middle of the triphenylene unit whereas for the PPP chain the pattern is the same but arbitrary.

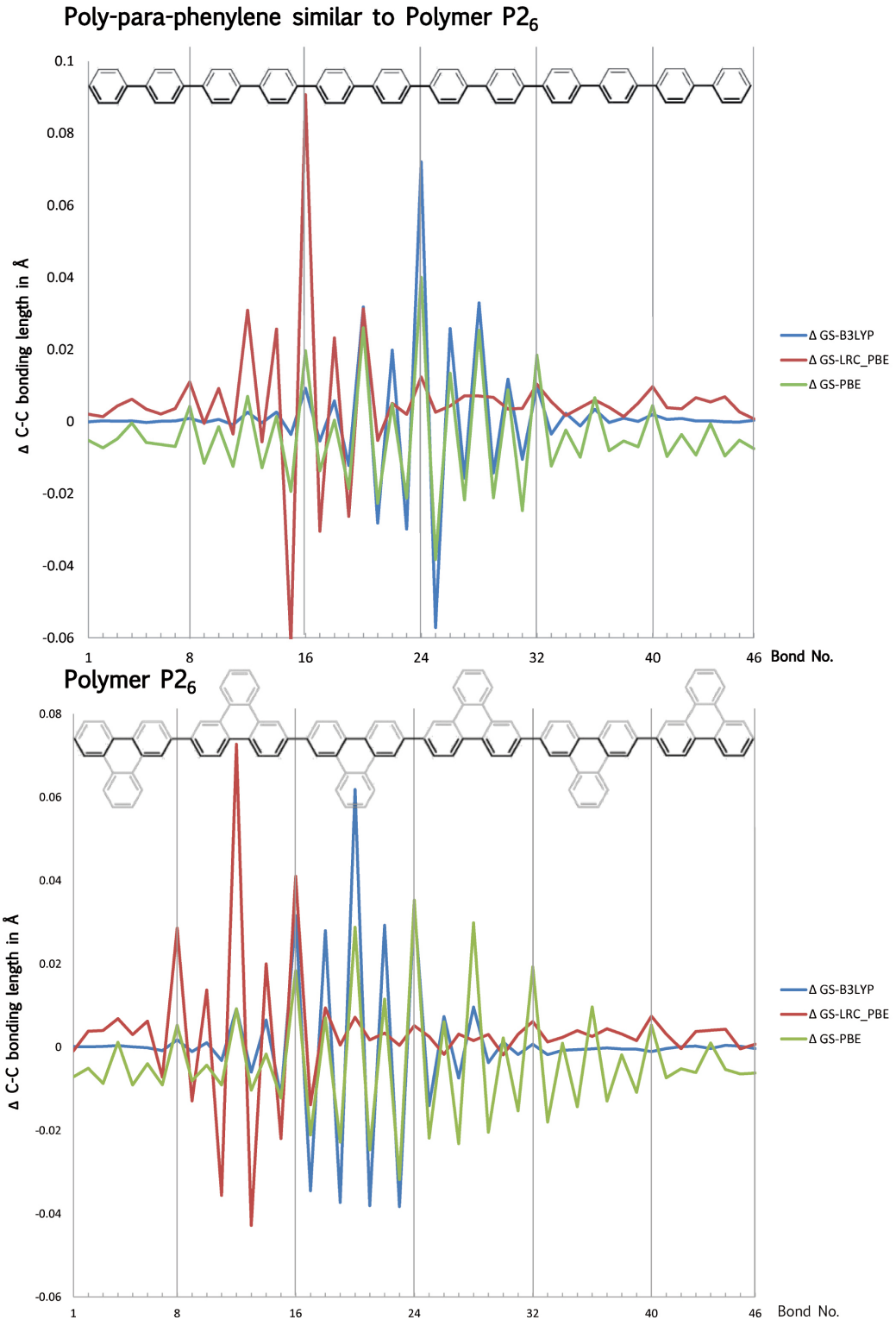

Figure 27: The triplet localization of the poly-para-phenylene (PPP) chain corresponding to $P2_6$ is very similar to the localization of $P2_6$

Additionally, the TDDFT energies for B3LYP and LRC-PBE are very similar as shown in the next table - estimations of emission energies could therefore also been made with PPP instead of the full triphenylene based chain.

	PBE		**B3LYP**		**LRC-PBE**	
	Abs.	Emiss.	Abs.	Emiss.	Abs.	Emiss.
			PPP_{12}			
S1	2.72		3.38		3.82	
T1	2.50	2.34	2.75	2.13	2.95	2.32
			$P2_6$			
S1	2.58		3.22		3.59	
T1	2.39	1.97	2.68	2.14	3.87	2.31

Table 5: Absorption and emission energies in eV for the pure poly-para-phenylene (PPP) chain with 12 units with the very similar triphenylene chain $P2_6$ (see Sec. 3.2). The absorption energies are different, but the phosphorescence energy is almost identical using B3LYP or LRC-PBE.

3.12 Discussion of the Deviating Results

The phosphorescence energies resulting from TDDFT vary by more than 1 eV for different polymer types whereas in experiment this energy is nearly fixed (see Fig. 17). It seems that the different localization behavior (localization around the 'bridging units' instead of the triphenylene units) accounts for this (see Sec. 3.11). This deviating localization pattern can have different reasons.

First, the neglected outer benzol rings that are bound to all triphenylene units in the experiment (visualized in M1; in P2 these rings are missing, see Fig. 5) - the inclusion of these could lead due to more electron-electron interactions to a localization on the triphenylene units instead on the bridging units in between.

Second, the optimized triplet geometry could describe a local minimum that is not the 'true' excited state geometry - this global minimum could be the localization on a triphenylene unit. This could be tested by starting the triplet geometry optimization from such a 'guessed' localization and see whether the localization stays there and whether the total energy of this conformation is lower than the one resulting from a 'normal' run.

Another thing that could explain the discrepancy is that the measured triplet state in experiment is not necessarily the lowest triplet excited state. It could also be the emission from a higher excited triplet state, with a different localization pattern than the lowest

triplet. Kasha's rule is sometimes ignored[106],[106] and in most phosphorescence experiments the level of the triplet emitting state is not explicitly checked. However, strong oscillator strengths lead predominantly to the suggestion, that the radiation is emitted by the lowest triplet excited state.
Additionally the Van-der-Waals interactions between the different polymer chains in the polystyrene matrix could lead to effects that are not negligible - this is out of reach for a description with DFT for molecules - one would have build the polymer as periodic system like a solid.

4 Summary and Outlook

The goal of this work was to reproduce the main results of the experiment performed by the group of Lupton[9] by means of TDDFT. The core message was that the singlet-triplet gap can be tuned by choosing different types of triphenylene based polymers. Yet, the results from the TDDFT calculations do not emphasize this observation. The phosphorescence energies vary by more than 1 eV instead of the observed value of 2.37 eV which is almost unique for all kind of examined polymers. The reason for this discrepancy is found in a different localization pattern of the first triplet excited state. Instead of localizing always on a triphenylene unit, what would explain the almost 'fixed' triplet energy, the localization happens on the bridging units in between the triphenylene units leading to varying phosphorescence energies. Reasons for this different behavior may lie in the neglect of the full polymer structure or triplet geometries that are not converged into a global minima. Van-der-Waals forces may also play an role or the examined triplet state in experiment could be a higher excited state.

Yet, the results are still useful and sensible. First, the improvement by the use of long-range corrected XC functionals is obvious. The localization pattern is clear, the phosphorescence energies have the highest accuracy when compared to experiment and the S-T gap converges a finite value. The use of this LRC XC functionals however, requires a time demanding pre-tuning of the γ parameter (as described in Sec. 2.12) that differs for each polymer.

A lower level of sophistication that is still acceptable but computationally faster can be reached by use of the global hybrid B3LYP. The localization behavior is very similar to the LRC XC functional results what is due to the use of an fraction of HF exchange in both functionals and the results for excitation energies and the S-T gap are similar but not so accurate.

The semilocal XC functional PBE however can not be suggested for trustworthy transition energies, triplet geometry optimizations or the localization behavior. Transition energies are much too low, singlet-triplet gaps converge to zero and the triplet excited state geometry optimizations reach a state where the 0-0 energy is often incorrect, indicating a geometry that is not converged. This shows the fundamental improvement between the inclusion of the LRC corrected semilocal XC functional (LRC-PBE) and the basic semilocal XC functional (PBE) which are basically the same.

The experiment of the group of Lupton[9] indicated that the singlet-triplet gap can be tuned by incorporating different types of 'bridging' units into the triphenylene backbone. The long-term goal would be to produce with TDDFT accurate results for this singlet-triplet

gap - in order to pre-tune the gap just by varying the geometries and molecules in the computer code. However, this accuracy is not yet reached because the localization patterns and phosphorescence energies differ as shown in this work. Still, TDDFT is a important tool to support experiments. Calculated results can be systematically improved by using range-separated XC functionals. This could be a motivation to develop the up-to-now very time consuming pre-tuning of the LRC γ parameter by means of theory (to get a good initial guess) and more sophisticated computer codes.
Overall, range-separated TDDFT calculations of conjugated polymers may help to discover potential device applications, f.e. in organic light-emitting diodes (OLEDs).

5 Appendix

The following tables show all kind of calculated excitation energies: Absorption, 0-0 energy and emission. Emission energies could mostly only be gained for the phosphorescence as explained in Sec. 3.4 - the experimental phosphorescence value for each polymer is roughly 2.37 eV.
Only the planar polymer 2 and polymer 6 yielded fluorescence energies - the experimental fluorescence value of $P2$ is 3.1 eV and 2.4 eV for $P6$.
Calculations that did not converge or finish are marked with 'not conv.' - the 0-0 energy is than consequently also missing. If the 0-0 energy is not located between absorption and emission, this indicates, that the total energy of the triplet optimized geometry is not converged into a global minima - the triplet emission energy is consequently useless. This wrong behavior occurs only if the PBE XC functional is used.
Attached to this master thesis there is also a DVD containing all input and output files for the DFT and TDDFT calculations, all resulting geometries and excitation energies, carbon-carbon bonding length tables and all relevant plots.

5.1 Polymer 2 (Triphenylene)

Table 6: Absorption, 0-0 energy and emission for polymer 2 in eV; twisted structure. (The S2 was taken as the lowest excited singlet state if the oscillator strength was larger than for S1. All S1 and S2 values for the relevant polymers concerning oscillator strength are listed in Table 12.)

	PBE			**B3LYP**			**LRC-PBE**		
	Abs.	0-0	Emiss.	Abs.	0-0	Emiss.	Abs.	0-0	Emiss.
				$P2_1$ (Triphenylene)					
S1	3.67			4.02			4.26		
T1	3.16	3.03	2.93	3.20	3.14	2.99	3.34	3.33	3.16
				$P2_2$					
S1	3.34 (S2)			3.84 (S2)			4.03 (S2)		
T1	2.78	2.33	2.09	2.95	2.59	2.14	3.13	2.74	2.30
				$P2_3$					
S1	3.00			3.54			3.90 (S2)		
T1	2.54	2.52	1.99	2.82	2.14	2.10	3.00	2.68	2.29
				$P2_4$					
S1	2.80			3.40			3.76		
T1	2.51	2.05	1.95	2.77	2.48	2.06	2.95	2.57	2.22
				$P2_5$					
S1	2.69			3.32			3.68		
T1	2.46	1.94	1.96	2.74	2.34	2.12	2.92	2.33	2.31
				$P2_6$					
S1	2.58			3.22			3.59		
T1	2.39	1.95	1.97	2.68	2.48	2.14	2.87	2.53	2.31
				$P2_7$					
S1	2.58			3.24			3.61		
T1	2.42	1.94	1.98	2.72	2.51	2.14	2.90		not conv.
				$P2_8$					
S1	2.50			3.18			3.55		
T1	2.37		not conv.	2.67		not conv.	2.86	2.44	2.31

5.2 Polymer 3

Table 7: Absorption, 0-0 energy and emission for polymer 3 in eV; twisted structure. (The S2 was taken as the lowest excited singlet state if the oscillator strength was larger than for S1. All S1 and S2 values for the relevant polymers concerning oscillator strength are listed in Table 12.)

	PBE			**B3LYP**			**LRC-PBE**		
	Abs.	0-0	Emiss.	Abs.	0-0	Emiss.	Abs.	0-0	Emiss.
					$P3_1$				
S1	3.11			3.93 (S2)			4.35 (S2)		
T1	2.76	2.40	2.16	3.04	2.71	2.23	3.21	2.89	2.14
					$P3_2$				
S1	2.66			3.42			3.70		
T1	2.41	2.00	1.86	2.75	2.41	2.14	2.88	2.43	2.00
					$P3_3$				
S1	2.41			3.21			3.58		
T1	2.26	1.87	1.84	2.68	2.38	1.98	2.85	2.37	2.13
					$P3_4$				
S1	2.31			3.15			3.47		
T1	2.22	1.79	1.82	2.67	2.38	1.99	2.80	2.27	2.11
					$P3_5$				
S1	2.30			3.13			3.48		
T1	2.22	1.74	1.84	2.67	2.44	2.02	2.82	2.20	2.12
					$P3_6$				
S1	2.25			3.12			not conv.		
T1	2.20	1.71	1.85	2.66	2.42	2.01	not conv.		not conv.

5.3 Polymer 4

Table 8: Absorption, 0-0 energy and emission for polymer 4; planar structure. Some triplet emission energies yielded negative values (marked with 'neg') - indicating, that the triplet excited geometry has a lower energy than the ground state. Therefore the ground state needs to be converged again into a lower total energy state - this was in many cases performed but not every calculation did finish.

	PBE		**B3LYP**		**LRC-PBE**	
	Abs.	Emiss.	Abs.	Emiss.	Abs.	Emiss.
			$P4_1$			
S1	2.85		3.41		3.65	
T1	3.41	1.71	2.42	1.93	2.54	1.84
			$P4_2$			
S1	2.11		2.75		3.07	
T1	1.80	1.45	2.15	1.66	2.28	1.74
			$P4_3$			
S1	1.85		2.59		3.01	
T1	1.71	neg.	2.09	neg.	2.28	neg.
			$P4_4$			
S1	1.75		2.52		2.94	
T1	1.67	1.41	2.07	not conv.	2.26	1.76
			$P4_5$			
S1	not conv.		not conv.		not conv.	
T1	not conv.	not conv.	not conv.	not conv.	not conv.	not conv.
			$P4_6$			
S1	1.53		2.47		2.87	
T1	1.45	not conv.	2.06	not conv.	2.24	not conv.

5.4 Polymer 5

Table 9: Absorption, 0-0 energy and emission for polymer 5 in eV; planar structure.

	PBE			**B3LYP**			**LRC-PBE**		
	Abs.	0-0	Emiss.	Abs.	0-0	Emiss.	Abs.	0-0	Emiss.
					$P5_1$				
S1	2.62			3.20			3.47		
T1	1.89		1.39	2.10	1.79	1.40	2.23	1.86	1.45
					$P5_2$				
S1	1.88			2.58			2.85		
T1	1.60	1.24	1.20	1.86	1.61	1.25	1.98	1.61	1.34
					$P5_3$				
S1	1.67			2.37			2.69		
T1	1.50	1.10	1.16	1.80	1.58	1.23	1.94	1.53	1.33
					$P5_4$				
S1	1.61			2.30			2.67		
T1	1.47		not conv.	1.79	1.58	1.24	1.94	1.48	1.32
					$P5_5$				
S1	1.55			2.27			2.61		
T1	1.46	0.96	1.15	1.78	1.57	1.22	1.92		not conv.
					$P5_6$				
S1	1.53			2.25			not conv.		
T1	1.45		not conv.	1.77	1.60	1.22	not conv.		not conv.

5.5 Polymer 6

Table 10: Absorption, 0-0 energy and emission for polymer 6 in eV; planar structure.

	PBE			**B3LYP**			**LRC-PBE**		
	Abs.	0-0	Emiss.	Abs.	0-0	Emiss.	Abs.	0-0	Emiss.
				$P6_1$					
S1	2.90			3.28			3.56		
T1	1.86	1.45	1.25	1.95	1.60	1.17	2.11	1.72	1.27
				$P6_2$					
S1	2.00			2.52			2.86		
T1	1.53	1.14	1.06	1.70	1.40	1.01	1.85	1.45	1.11
				$P6_3$					
S1	1.71			2.30			2.67		
T1	1.44	1.02	1.03	1.65	1.39	1.00	1.81	1.38	1.11
				$P6_4$					
S1	1.59			2.20			2.60		
T1	1.40	0.95	1.03	1.63	1.37	1.00	1.80	1.33	1.11
				$P6_5$					
S1	1.56			2.20			2.60		
T1	1.41	0.91	1.04	1.64	1.38	1.00	1.81	1.28	1.12
				$P6_6$					
S1	1.51			2.18			2.65		
T1	1.41	0.85	1.04	1.64	1.38	1.00	1.83	1.24	1.12

5.6 Excitation Energy Comparison of Planar and Twisted Geometries

Table 11: S1/T1 absorption (abs.) and emission (emiss.) energies in eV for polymer 2 from $n = 1$ to $n = 6$. The experimental fluorescence value for this kind of polymer is 3.04 eV and the phosphorescence is 2.39 eV (for chain lengths varying between $n = 11$ and $n = 200$). S1 emission energies based on the relaxed S1 geometry could only be calculated for planar structures in *ADF*, where the XC functional B3LYP was used

	Twisted						**Planar**					
	PBE		**B3LYP**		**LRC-PBE**		**PBE**		**B3LYP**		**LRC-PBE**	
	abs.	emiss.	abs.	emiss.	abs.	emiss.	abs.	emiss.	abs.	emiss.	abs.	emiss.
$P2_1$ (Triphenylene)												
S1							3.67		4.02	3.72	4.26	
T1							3.16	2.93	3.20	2.99	3.34	3.16
$P2_2$												
S1	3.32		3.82		4.02		3.19		3.68	3.49	3.90	
T1	2.78	2.09	2.95	2.14	3.13	2.30	2.60	2.31	2.77	2.47	2.94	2.29
$P2_3$												
S1	3.00		3.54		3.88		2.81		3.30	2.96	3.63	
T1	2.54	1.99	2.82	2.10	3.00	2.29	2.36	2.09	2.59	2.34	2.77	2.23
$P2_4$												
S1	2.80		3.40		3.76		2.58		3.12	2.79	3.47	
T1	2.51	1.95	2.77	2.06	2.95	2.22	2.25	1.84	2.51	2.02	2.71	2.18
$P2_5$												
S1	2.69		3.32		3.68		2.44		3.02	2.71	3.39	
T1	2.46	1.96	2.74	2.12	2.92	2.31	2.19	1.85	2.48	2.01	2.68	2.50
$P2_6$												
S1	2.58		3.22		3.59		2.35		2.96	2.68	3.32	
T1	2.39	1.97	2.68	2.14	2.87	2.31	2.15	1.83	2.45	2.00	2.65	2.18

5.7 Energies, Oscillator Strengths and Orbital Mixing of the Two Lowest Excited Singlet States

Table 12: S1 and S2 energies in eV, oscillator strength f and the orbital mixing of the transition. The listed monomer $M1$, polymers $P2$ and $P3$ show that the S2 and S1 is sometime switched depending on the functional and polymer. We chose the transition with the highest oscillator strength to be the lowest singlet excited state, see also Sec. 3.6

	PBE			**B3LYP**			**LRC-PBE**		
	Abs.	f	orbitals	Abs.	f	orbitals	Abs.	f	orbitals
				$M1$					
S1	3.18	3.176	H->L+1, H-1->L	3.76	0.010	H->L+1, H-1->L	3.88	0.005	H->L+1, H-1->L
S2	3.19	0.116	H -> L	3.84	0.116	H -> L	4.12	0.122	H -> L
				$P2_2$					
S1	3.32	0.000	H->L+1, H-1->L	3.82	0.000	H->L+1, H-1->L	4.02	0.000	H->L+1, H-1->L
S2	3.34	0.148	H -> L+2, H-> L	3.84	0.749	H -> L	4.03	0.002	H -2-> L, H-> L+2
				$P2_3$					
S1	3.00	1.195	H -> L	3.54	1.969	H->L	3.88	0.000	H-4 -> L, H -> L+2
S2	3.13	0.001	H->L+1, H-1->L	3.71	0.000	H-4 -> L, H -> L+1	3.90	2.382	H -> L
				$P3_1$					
S1	3.11	0.060	H-> L	3.86	0.001	H-1-> L+1, H-2 -> L	4.18	0.000	H->L+1, H-1->L
S2	2.76	0.030	H-1->L, H->L	3.93	0.337	H->L	4.35	0.478	H->L

References

[1] F. Jensen, John Wiley & Sons Ltd, Second Edition (2007).

[2] S. Boti, A. Schidlmayr, R. D. Sole, L. Reining, Rep. Prog. Phys. 70, 357-407 (2007).

[3] E. K. U. Gross, N. T. Maitra, Springer, Lecture Notes in Physics Vol. 837 (2012).

[4] A. Dreuw, M. Head-Gordon, Chem. Rev. 105, 4009-4037 (2005).

[5] M.A. L. Marques, A. Rubio, Time-dependent density functional theory, edited by M.A.L. Marques, C.A. Ullrich, F. Nogueira, A. Rubio, K. Burke, E.K.U. Gross, Springer, Berlin Heidelberg (2006).

[6] A. C. Grimsdale, K. L. Chan, R. E. Martin, P.G. Jokisz, A. B. Holmes, Chem. Rev. 109, 897 (2009).

[7] B. Milian-Medina, J. Gierschner, Elsevier B.V. Vol. 13, 6, 939-1120 (2012).

[8] a) M. A. Baldo, D. F. O'Brien, Y. You, A. Shoustikov, S. Sibley, M. E. Thompson, S. R. Forrest, Nature, 395, 151 (1998); b) V. Cleave, G. Yahioglu, P. Le Barny, R.H. Friend, N. Tessler, Adv. Mater.11, 285 (1999); c) X.H. Yang, D. C. Müller, D. Neher, K. Meerholz, Adv. Mater. 18, 948 (2006); d) L.Ying, A.Q. Zhang, W. Yang, Y. Cao, Prog. Chem. 21, 1275 (2009); e) S. Haneder, E. Da Como, J. Feldmann, J.M. Lupton, C. Lennartz, P. Erk, E. Fuchs, O. Molt, I. Münster,C. Schildknecht, G. Wagenblast, Adv. Mater. 20, 3325 (2008); f) H. Yersin, Top. Curr. Chem. 241,1 (2004).

[9] D. Chaudhuri, H. Wettach, K.J. van Schooten, S. Liu, E. Sigmund, S. Höger, J.M. Lupton, Angew. Chem. Int. Ed. 49, 7714 (2010).

[10] R. Baer, E. Livshits, U. Salzner, Annual Review of Physical Chemistry. 61, 85-109 (2010).

[11] M. A. Rohrdanz, J. M. Herbert, J. Chem. Phys. 129, 034107 (2008).

[12] F. Schwabl, Springer Berlin Heidelberg (2002).

[13] M. Born, R. Oppenheimer, Annalen der Physik 389, Vol. 20, 457–484 (1927).

[14] J. P. Perdew, M. Levy, Phys. Rev. Let. 51, 20 (1983).

[15] A. J. Cohen, P. M.-S. and W. Yang, Science 321, 5890, 792-294 (2008).

[16] P. Elliott, K. Burke, F. Furche, arXiv:cond-mat/0703590 (2007).

[17] E.K.U. Gross, K. Burke, Springer-Verlag Berlin Heidelberg, Lect. Notes Phys. 706, 1–17 (2006).

[18] R. G. Parr, W. Yang, Oxford University Press, 1989; L. J. Bartolotti, K. Flurchick, Rev. Comp. Chem., 7, 187 (1996); A. St-Amant, Rev. Comp. Chem., 7, 217 (1996); T. Ziegler, Chem. Rev., 91, 651 (1991); E. J. Baerends, O.V. Gritsenko, J. Phys.Chem., 101, 5383 (1997).

[19] W. Koch, M. C. Holthausen, Wiley-VCH (2000).

[20] P.-O. Löwdin, Int. J. Quant. Chem., 19 (1986).

[21] P. Hohenberg,W. Kohn, Phys. Rev., 136, B864 (1964).

[22] M. Levy, Phys. Rev. A 26, 1200 (1982).

[23] W. Kohn, L. J. Sham, Phys. Rev., 140, A1133 (1965).

[24] M. Elstner, D. Porezag, G. Jungnickel, T. Frauenheim, S. Suhai, G. Seifert, edited by P. E. A. Turchi, A. Gonis, L. Colombo, Materials Research Society, Pittsburgh, PA, Vol. 491, 131 (1991).

[25] E. K. U. Gross, W. Kohn, Adv. Quantum Chem. 21, 255 (1990).

[26] A.D. Becke, Phys. Rev. A 38, 3098 (1988).

[27] C. Lee, W. Yang, R.G. Parr, Phys. Rev. B 37, 785 (1988).

[28] A.D. Becke, J. Chem. Phys. 98, 1372–1377 (1993).

[29] P. J. Stephens, F. J. Devlin, C. F. Chabalowski, M. J. Frisch, J. Phys. Chem. 98, 11623–11627 (1994).

[30] C. Adamo, V. Barone, J. Chem. Phys. 110, 6158-69 (1999).

[31] J. P. Perdew, K. Burke, M. Ernzerhof, Phys. Rev. Lett., 77, 3865-68 (1996).

[32] J. P. Perdew, K. Burke, M. Ernzerhof, Phys. Rev. Lett., 78, 1396 (1997).

[33] E. Livshits, R. Baer, Phys. Chem. Chem. Phys. 9, 2932–41(2007).

[34] M. Levy, Proc. Natl. Acad. Sci. USA 76, 6062– 65 (1979).

[35] A. Seidl, A. Gorling, P. Vogl, J.A. Majewski, M. Levy, Phys. Rev. B 53, 3764–74 (1996).

[36] C.-O. Almbladh, U. v. Barth, Phys. Rev. B 31, 3231–44 (1985).

[37] not conv. Handy, M.T. Marron, H.J. Silverst 1969, Phys. Rev. 180,45–48 (1969).

[38] I.C. Gerber, J.G. Angyan., Chem. Phys. Lett. 415,100–105 (2005).

[39] T. Leininger, H. Stoll, H.-J. Werner, A. Savin, Chem. Phys. Lett. 275, 151–160 (1997).

[40] M. Thiele, E.K.U. Gross, S. Kümmel, Phys. Rev. Lett. 100,153004 (2008).

[41] R. Baer, arXiv:0808.3848v1 (2008).

[42] A. Dreuw, J. L. Weisman, M. Head-Gordon, J. Chem. Phys. 119, 2943 (2003).

[43] E. P. Fowe, A. D. Bandrauk, ed. by F. J. Duarte, InTech (2010).

[44] E. Runge, E.K.U. Gross, Phys. Rev. Lett. 52, 997 (1984).

[45] K.L. Liu, S.H. Vosko, Can. J. Phys. 67, 1015 (1989).

[46] E. Engel, R. M. Dreizler, Springer (2011).

[47] C. Guet, P. Hobza, F. Spiegelmann, F. David, Springer jointly published with EDP Sciences, Les Ulis (2001).

[48] A. van de Walle, G. Ceder, Phys. Rev. B 59, 23 (1999).

[49] D. Joubert, Springer Berlin Heidelberg, (1998).

[50] R. A. van Santen, P. Sautet, Wiley-VCH (2009).

[51] A. F. Izmaylov, G. E. Scuseria, J. Chem. Phys. 129, 034101 (2008).

[52] Y. Tawada, T. Tsuneda, S. Yanagisawa, T. Yanai, K. Hirao, J. Chem. Phys. 120, 8425 (2004).

[53] E. K. U., W. Kohn, 1985, Phys. Rev. Lett. 55, 2850–2852; ibid, 57, 923(E) (1986).

[54] Petersilka, M., U. J. Gossmann, E. K. U. Gross, Phys. Rev. Lett. 76, 1212–1215 (1996).

[55] Casida, M.E., in Recent Developments and Application of Modern Density Functional Theory,edited by J.M. Seminario Elsevier Amsterdam, 391–439 (1996).

[56] M. E. Casida, Recent Advances in Density Functional Methods, edited by D.E. Chong, Vol. 1 of Recent Advances in Computational Chemistry, pp. 155–192 (1995).

[57] J.R. Chelikowsky, Y. Saad, I. Vasiliev, Springer-Verlag Berlin Heidelberg, Lect. Notes Phys. 706, 259-269 (2006).

[58] Rubio,A.,J.A.Alonso, X.Blase,L.C.Balbás, S. G. Louie, Phys. Rev. Lett. 77, 247–250; Phys. Rev. Lett. 77, 5442(E) (1996).

[59] Görling, A., Phys. Rev. Lett. 83, 5459–5462.

[60] Furche, F., K. Burke, Annual Reports in Computational Chemistry 1, edited by D. Spellmeyer, Elsevier Amsterdam, 19–30 (2005).

[61] K. Burke, J. Werschnik, E. K. U. Gross, J. Chem. Phys. 123, 0622061 (2005).

[62] T. Körzdörfer, J. S. Sears, C. Sutton, J.-L. Brédas, J. Chem. Phys. 135, 204107 (2011).

[63] H. Haken, H. C. Wolf, Springer, 5.Auflage (2006).

[64] a) J. S.Wilson, A. Köhler, R.H. Friend, M. K. Al-Suti, M. R. A. Al-Mandhary, M. S. Khan, P. R. Raithby, J. Chem. Phys. 113, 7627 (2000); b) D.Wasserberg, P. Marsal, S. C. J. Meskers, R. A. J. Janssen, D. Beljonne, J. Phys. Chem. B 109, 4410 (2005); c) A. Köhler, D. Beljonne, Adv. Funct. Mater. 14, 11 (2004); d) A. Köhler, J. S. Wilson, R. H. Friend, Adv. Mater. 14, 701 (2002); e) A. Köhler, J. S. Wilson, R. H. Friend, M. K. Al-Suti, M. S. Khan, A. Gerhard, H. Bässler, J. Chem. Phys. 116, 9457 (2002); f) D. Beljonne, Z. Shuai, G. Pourtois, J. L. Brédas, J. Phys. Chem. A 105, 3899 (2001); g) P. C. Jha, E. Jansson, H. Agren, Chem. Phys. Lett. 424, 23 (2006); h) L. P. Chen, L. Y. Zhu, Z. G. Shuai, J. Phys. Chem. A 110, 13349 (2006); i) J. J. Apperloo, C. Martineau, P. A. van Hal, J. Roncali, R. A. J. Janssen, J. Phys. Chem. A 106, 21 (2002); j) F. Laquai, C. Im, A. Kadashchuk, H. Bässler, Chem. Phys. Lett. 375, 286 (2003).

[65] a) J. Schmidt, W. G. Vandorp, J. H. van der Waals, Chem. Phys. Lett. 8, 345; (1971) b) J. Langelaar, R. P.H. Rettschnick, A. M. F. Lamrooy, G. J. Hoytink, Chem. Phys. Lett. 1, 609 (1968); c) N. Nishi, K. Matsui, M. Kinoshita, J. Higuchi, Mol. Phys. 38,1 (1979); d) D. A. Antheunis, J. Schmidt, J. H. van derWaals, Chem. Phys. Lett. 6, 255 (1970); e) D. Baunsgaard, M. El Balsami, J. Frederiksen,N. Harrit, F. Negri, G. Orlandi, R. Wilbrandt, Laser Chem. 19, 349 (1999); f) W. D. K. Clark, A.D. Litt, C. Steel, J. Am. Chem. Soc. 91, 5413 (1999); g) R. E. Kellogg, R. G. Bennett, J. Chem. Phys. 41, 3042 (1964); h) A. A. Lamola, G. S. Hammond, J. Chem. Phys. 43, 2129 (1965).

[66] Conjugation of the building blocks is confirmed by considering an oligomer series of 2, which reveals a bathochromic shift in fluorescence and absorption. No lower-lying triplet emissions are seen in any of the low-exchange-gap samples. See the Supporting Information of[9] for further details and spectra.

[67] a) T. Dutta, K. B. Woody, S. R. Parkin, M.D. Watson, J. Gierschner, J. Am. Chem. Soc. 131, 17321 (2009); b) K. Glusac, M. E. Kose, H. Jiang, K. S. Schanze, J. Phys. Chem. B 111, 929 (2007).

[68] E.J. Baerends, V. Branchadell, M. Sodupe, Chemical Physics Letters 265,481 (1997).

[69] F. M. Bickelhaupt, E. J. Baerends, in Reviews of Computer Chemistry, edited by K. B. Lipkowitz, D. B. Boyd, Wiley-VCH, New York, 1-86 (2000).

[70] M. Elstner, D. Porezag, G. Jungnickel, J. Elsner, M. Haugk, Th. Frauenheim, S. Suhai, G. Seifert, Phys. Rev. B 58, 7260 (1998).

[71] T. Frauenheim, G. Seifert, M. Elstner, Z. Hajnal, G. Jungnickel, D. Porezag, S. Suhai, R. Scholz, Phys. Stat. Sol. (b) 217, 41 (2000).

[72] M. Valiev, E.J. Bylaska, N. Govind, K. Kowalski, T.P. Straatsma, H.J.J. van Dam, D. Wang, J. Nieplocha, E. Apra, T.L. Windus, W.A. de Jong, Comput. Phys. Commun. 181, 1477 (2010).

[73] Molecular Sciences Software Group, NWChem User Dokumentation Release 5.1 (2007).

[74] D. Jacquemin, V. Wathelet, E. A. Perpete, C. Adamo, J. Chem. Theory Comput.5, 2420 (2009).

[75] D. Jacquemin, E. A. Perpete, I. Ciofini, C. Adamo, J. Chem. Theory Comput. 6, 1532 (2010).

[76] S. Hirata, M. Head-Gordon, R. J. Bartlett, J. Chem. Phys. 111, 10774 (1999).

[77] Y.-L. Wang, G.-S. Wu, J. Quant. Chem. 108, 430 (2007).

[78] A. Pogantsch, G. Heimel, E. Zojer, J. Chem. Physk. 117, 5921 (2002).

[79] G. Mao, J. E. Fischer, F. E. Karasz, M. J.Winokur, J. Chem. Phys. 98, 712 (1993).

[80] B. M. Wong, T. H. Hsieh, J. Chem. Theory Comput. 6, 3704 (2010).

[81] S. Grimme, M. Parac, Chem. Phys. Chem. 3, 292 (2003).

[82] S. Hirata, M. Head-Gordon, Chem. Phys. Let. 314, 291 (1999).

[83] W. Barford, Oxford University Press, International Series of Monographs in Physics 129 (2005).

[84] R. M. Richard, J.M. Herbert, J. Chem. Theory Comput. 7, 1296 (2011).

[85] M. J. Peach, P. Benfield, T. Helgaker, D. J. Tozer, J. Chem. Phys. 128, 044118 (2008).

[86] N. Kuritz, T. Stein, R. Baer, L. Kronik, J. Chem. Theory Comput. 7, 2408 (2011).

[87] J. S. Sears, Th. Koerzdoerfer, C.-R. Zhang, J.-L. Brédas, J. Chem. Phys 125, 151103 (2011).

[88] S. Sok, S. Y. Willow, F. Zahariev, M. S. Gordon, J. Phys. Chem. A 115, 9801 (2011).

[89] Y. Tawada, T. Tsuneda, S. Yanagisawa, J. Chem. Phys. 120, 8425 (2004).

[90] W. Thomas, Naturwissenschaften 13, 625 (1925).

[91] F. Reiche, W. Z. Thomas, Phys. 34, 510 (1925).

[92] W. Z. Kuhn, Phys. 33, 408 (1925).

[93] M. E. Casida, In Recent Advances in Density Functional Methods, Part I, D. P. Chong, Ed., World Scientific: Singapore, 155 (1995).

[94] S. Tretiak, K. Igumenshchev, V. Chernyak, Phys. Rev. B 71, 033201 (2005).

[95] J. N. Murrell, London: Chapman and Hall (1963).

[96] L. Salem, W. A. Benjamin, New York (1966).

[97] J. R. Platt, J. Chem. Phys. 25, 80 (1956).

[98] L. G. S. Brooker, G. H. Keyes, D. W. Heseltine, J. Am. Chem. Soc. 73, 1951 (1951).

[99] A. A. Ovchinnikov, C. H. Ukrainskii, G. V. Kventsel, Sov. Phys. Usp. 15, 575 (1973).

[100] F. Bar, W. Huber, G. Handsching, H. Martin, H. Kuhn, J. Phys. Chem. 32, 470 (1960).

[101] H. Labhart, J. Chem. Phys. 27, 957 (1957).

[102] Y. Ooshika, Phys. Soc. Jpn. 12, 1238, 1246 (1957).

[103] J. M. Andree', G. LeRoy, Theor. Chim. Acta 9, 123 (1967).

[104] J. Ma, S. Li, Y. Jiang, Macromolecules 35, 1109 (2002).

[105] B. Wardle,Wiley (2009).

[106] N. J. Turro, V. Ramamurthy, J.C. Scaiano, University Science Books, Sausalito, CA, (2008).